Collective and two-quasiparticle excitations in $^{102,104,106}Pd$ following (^{13}C, $3n\gamma$) reactions*

J. A. Grau, L. E. Samuelson, F. A. Rickey, P. C. Simms, and G. J. Smith†

Tandem Accelerator Laboratory, Purdue University, Lafayette, Indiana 47907

(Received 29 March 1976)

Even-A Pd nuclei were studied using the reactions $^{92,94,96}Zr(^{13}C, 3n\gamma)^{102,104,106}Pd$. The experiments included γ-ray yield as a function of energy, γ-ray angular distributions, γ-ray linear polarizations, and γ-γ coincidence measurements. A new treatment of γ-γ directional correlation from oriented nuclei, which combines data from all appropriate coincidence pairs to reduce uncertainties, has aided in determining multipolarities for 49 contaminated transitions. Extensive decay schemes are presented which include many high-angular-momentum, positive- and negative-parity states. In addition to the ground-state band, there appear to be three collective bands built on excited two-quasiparticle states. The measurements favor a slightly deformed rotor description of these nuclei over an interpretation in terms of a vibrational (interacting boson) model.

[NUCLEAR STRUCTURE $^{92,94,96}Zr(^{13}C, 3n\gamma)$ $E = 45$–56 MeV; measured $I_\gamma(E(^{13}C))$, $I_\gamma(\theta)$, $\gamma\gamma$ coin, $\gamma\gamma$ DCO, P_γ. $^{102,104,106}Pd$ deduced levels, J, π, γ multipolarity.]

I. INTRODUCTION

Previous experiments[1] on $^{101,103,105}Pd$ and the present results for $^{102,104,106}Pd$ have shown that the *majority* of states populated by (HI,xn) reactions in Pd nuclei are members of decoupled collective bands built on quasineutron states. These nuclei provide an unusually simple and complete illustration of the relation between particle and collective motion in slightly deformed nuclei.

The particle-core interaction produces two dominant effects[1] in the odd-A nuclei $^{101,103,105}Pd$. (1) The yrast states usually have the angular momentum j of the odd particle aligned with the collective angular momentum R of the core, $I=j+R$. (Yrast states are preferentially populated in (HI,xn) reactions because they have minimum energy for a given total angular momentum I.) (2) The odd particle appears to be "decoupled" from the core, that is, the energy of excited states is approximately equal to the simple sum of the odd-particle energy plus the collective energy of the core as if the particle-core interaction were small. Decoupling has been observed in a variety of nuclei[2,3] where the odd particle is in a state with relatively high spin and pure j (e.g., $h_{11/2}$ and $i_{13/2}$ in the $N=4$ and 5 shells, respectively). However, these Pd nuclei are particularly interesting because decoupling has been observed[1] for states that have low spin and mixed j ($g_{7/2}$ and $d_{5/2}$) as well as the usual high-spin state ($h_{11/2}$).

In this paper we present a detailed analysis of the (HI,$xn\gamma$) experiments performed on $^{102,104,106}Pd$ showing that collective bands are also a dominant feature of the even-A Pd nuclei. In particular, the available two-quasineutron states involving combinations of $h_{11/2}$, $g_{7/2}$, and $d_{5/2}$ orbitals appear to decouple from the core motion as do the one-quasineutron states in $^{101,103,105}Pd$. States having spins 10^+, 9^-, and 8^-, which are the highest two-quasineutron spins possible from these orbitals, are strongly fed by collective bands similar in energy spacing to the ground-state bands of the core nuclei. In Sec. VI we will show that these results can be readily understood when the Pd nuclei are described as slightly deformed rotors.

The experiments included excitation functions, γ-ray angular distributions, γ-ray linear polarization measurements, and γ-γ coincidence measurements following the reactions $^{92,94,96}Zr$-$(^{13}C, 3n)^{102,104,106}Pd$. Our procedures for most of these experiments have been described previously.[4,5] This paper will emphasize a rigorous, quantitative analysis of the γ-γ coincidence data to confirm and establish energy levels, spin assignments, and γ-ray transition strengths. This type of analysis can be essential when complex spectra are involved.

Some of our results for ^{102}Pd have already appeared in the literature,[6,7] as have papers from other authors[8-10] on ^{102}Pd, ^{104}Pd, and ^{106}Pd. In addition many Ag and Rh decay studies[11-17] have been made on $^{102,104,106}Pd$ populating spins up to 6^+. In Ref. 6 an (α,$n\gamma$) reaction was used to populate spins only as high as 10^+; the two-quasiparticle band structure was not observed. In Ref. 7 the spin of the 9^- state was established by the first experimental application of the DCO (γ-γ directional correlation from oriented nuclei) technique. The present publication will elaborate upon this technique.

II. EXPERIMENTAL PROCEDURE

The γ-ray data were measured with Ge(Li) detectors having active volumes of 25 to 35 cm^3 and energy resolutions of 2.2 to 2.5 keV full width at half maximum (FWHM) at 1332 keV. The targets used were 3 mg/cm^2-thick rolled foils of separated $^{92,94,96}Zr$ isotopes. The ^{92}Zr and ^{94}Zr targets were essentially pure isotopes while the ^{96}Zr target included significant fractions of contaminating isotopes, a problem which will be discussed along with the results for ^{106}Pd.

Near the peak cross section of the desired $(^{13}C, 3n)$ reaction substantial contributions from three other reactions were always observed: $(^{13}C, 4n)$, $(^{13}C, \alpha 2n)$, and $(^{13}C, p2n)$. The production of high-spin states is improved when the incident projectile energy is set high in the $3n$ range. However, this also increases the interference from the $4n$ and $p2n$ reactions, so a compromise energy must be selected.

A. γ-γ coincidence measurements

The γ-γ coincidence data were taken with two Ge(Li) detectors positioned at 3 cm from the target. Compton scattering of γ rays from one detector into the other was reduced by placing lead absorbers inside and outside of the target chamber. Two-parameter data were accumulated event by event on magnetic tape by a PDP-15 computer. Two single-channel analyzer (SCA) gates were set on the output of a time-to-amplitude converter so the events could be tagged as either true-plus-chance or chance. The chance events were subtracted from the true-plus-chance before peak areas were determined. The projection spectra for each detector (all γ rays in one detector which are coincident with any γ ray in the other detector) were stored in the computer memory. 60 million events were accumulated for the ^{102}Pd run, 35 million for ^{104}Pd, and 130 million for ^{106}Pd.

The coincidence projection spectrum for the $^{96}Zr(^{13}C, 3n)^{106}Pd$ reaction is shown in Fig. 1. Such a spectrum is particularly useful because, in general, good coincidence information is available on any γ ray which shows up as a distinct peak in the spectrum. While only the ^{106}Pd γ rays are indicated in the figure, virtually every other peak has been positively identified by the coincidence data as coming from one of the contaminant reactions.

After the coincidence data were recorded the tapes were searched with digital gates set on each peak and corresponding background in the X detector. A skewed Gaussian function was fitted to the peaks in the X-detector projection spectrum to determine the fraction of a peak contained within its window and the fractions of neighboring peaks in the window. A spectrum from detector Y was constructed for each gate set on detector X. Up to 239 spectra could be assembled onto a magnetic disk in one pass through the tapes. The remaining data were stored on a second magnetic tape so they could be recovered without reading through all of the original data. Quantitative coincidence intensities were extracted from Y spectra by setting digital gates on peaks in the Y-projection spectrum and making the same corrections for true peak fractions and overlaps with neighboring gates that were made for the X spectrum. Finally, the results were corrected for detector efficiencies and arranged in a two-dimensional array of quantitative coincidence intensities and uncertainties.

If the coincidence data are to accurately reflect the intensity of each transition one must be careful to remove the angular dependence from the data. When the detectors are located at angles of $90°$ and $-30°$ with respect to the beam line, the average of the two coincidence areas associated with each pair of transitions is proportional to the true coincidence intensity to within 5% for most spin sequences. The commonly used pair of angles $90°$ and $-90°$ is especially poor in this respect since a coincidence between two dipoles is detected much more efficiently (by ~60%) than a coincidence between two quadrupoles. Detectors placed at $0°$ and $100°$ give almost as good an average coincidence rate as the $90°$ and $-30°$ locations. The $0°, 100°$ pair has the advantage of giving improved sensitivity for the DCO analysis described below.

B. Angular momentum analysis

Angular distributions were measured at nine evenly spaced angles from $-30°$ to $+90°$. A 2.5×10^{-3} cm-thick Au beam stop was placed immediately behind the target and a thin film of Au was evaporated onto the back of the target to stop the recoiling Pd nuclei. Even with this precaution we still observed Doppler broadening of the line shapes for some transitions from high energy states. Frequently the singles spectra are so complicated that it is not possible to correct for the events which are lost from the normal Gaussian peak at forward angles. A complete description of our procedures for measuring angular distributions and an example of Doppler-shift corrections are included in Ref. 5.

In complicated spectra such as these it is common to find that a large percentage of the γ-ray peaks contain unresolved doublets. For example, even with the 2.3-keV resolution present in these

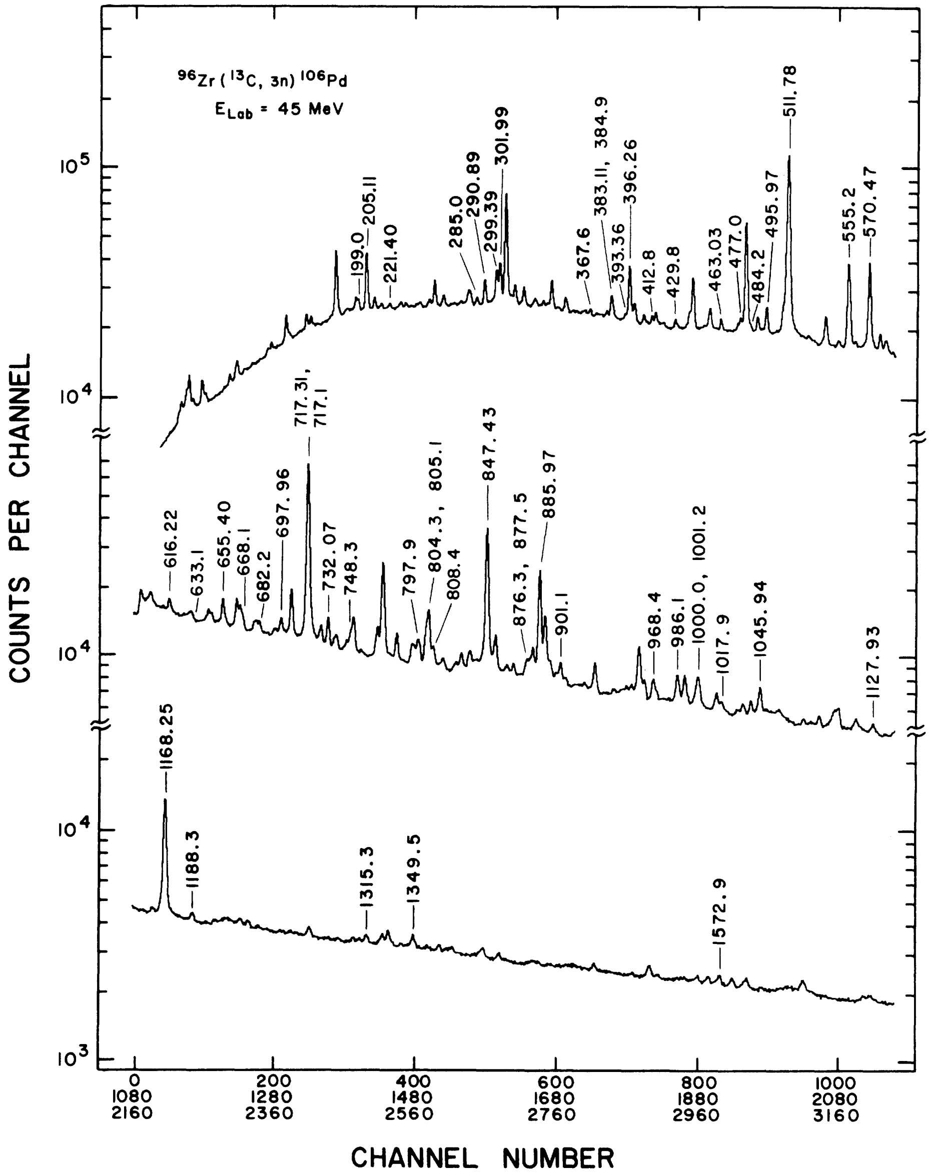

FIG. 1. Coincidence projection spectrum for ^{106}Pd. The data were accumulated during 40 hours of beam time with detectors positioned at 100° and 0°. The spectrum displayed is from the 100° detector, so that the very weak dipoles (e.g., 285.0) can be readily observed.

measurements, 21 out of the 48 γ rays assigned to ^{102}Pd are unresolved from other known γ rays and several others are suspected to be contaminated. Under these circumstances the singles angular distribution coefficients are actually weighted averages of the coefficients of the two competing γ rays, making it difficult or impossible to assign spins and parities on the basis of angular distributions.

The DCO method (γ-γ directional correlation from oriented nuclei) proposed by Krane, Steffen, and Wheeler[18] can overcome this difficulty by isolating the transition of interest in the coincidence data. Multipolarity information on the coincident γ rays can be extracted from the relation between the two coincidence intensities N_{12} and N_{21}, where N_{12} is the number of times γ_1 is detected in the X detector with γ_2 in the Y detector, and N_{21} is the number of times γ_2 is detected in X with γ_1 in Y:

$$R_{\rm DCO} \equiv \frac{N_{12}(\gamma_1 \to X, \gamma_2 \to Y)}{N_{21}(\gamma_2 \to X, \gamma_1 \to Y)}\,.$$

The interpretation of a DCO experiment is complicated since the ratio depends on the multipolarities of both γ_1 and γ_2. The interpretation can be simplified since the DCO ratio is approximately equal to the product of the γ-ray angular distributions:

$$R_{\mathrm{DCO}} \approx \frac{N(\gamma_1 \to X) N(\gamma_2 \to Y)}{N(\gamma_2 \to X) N(\gamma_1 \to Y)} = \frac{N(\gamma_1 \to X)/N(\gamma_1 \to Y)}{N(\gamma_2 \to X)/N(\gamma_2 \to Y)} = \frac{A(1)}{A(2)},$$

where $A(i)$ is the anisotropy of the γ rays for the detector positions used in the coincidence experiment. It is evident that we can obtain information about γ_1 only when $A(2)$ is known. This is easy when γ_2 is a quadrupole, but it is much harder when γ_2 can be a mixed transition. This complication can be avoided by comparing γ_2 to known quadrupole γ rays (γ_3). Then a corrected DCO ratio can be defined where the anisotropy of γ_1 is compared only to quadrupole transitions:

$$R_{\mathrm{DCOQ}} \approx \frac{A(1)}{A(2)} \frac{A(2)}{A(3)} = \frac{A(1)}{A(3)}.$$

Since the DCOQ ratio is determined primarily by the multipolarity of γ_1, much better statistical accuracy can be obtained by combining all DCOQ measurements involving the transition of interest. In terms of coincidence counting rates N_{ij}, the required correction factors can be defined as

$$\frac{a(\gamma_2)}{b(\gamma_2)} = \frac{\sum_{\gamma_3} N_{23}}{\sum_{\gamma_3} N_{32}},$$

with the additional requirement that $a + b = 2$ so $a = b = 1$ when γ_2 is quadrupole. Then the DCO ratio which is used to obtain information about γ_1 can be defined as

$$R_{\mathrm{DCOQ}}(\gamma_1) = \frac{\sum_{\gamma_2} a(\gamma_2) N_{12}(\gamma_1 \to X, \gamma_2 \to Y)}{\sum_{\gamma_2} b(\gamma_2) N_{21}(\gamma_2 \to X, \gamma_1 \to Y)}.$$

Measured values of this DCOQ ratio can readily be compared to theoretical predictions by calculating N_{12} and N_{21} using the DCO formalism outlined in Ref. 18. Each of these calculated intensities must be properly weighted by insisting that

$$(N_{12} + N_{21})_{\text{calculated}} = (N_{12} + N_{21})_{\text{measured}}.$$

The most important factor in the theoretical calculation of the DCOQ ratio is the total angular momentum change associated with the transition. The absolute value of I_i, I_f, and the orientation of the system will change the results only by 10 to 20%. Thus it is instructive to consider typical values of the DCOQ ratio as a function of the mixing ratio δ. Figure 2 shows the results for a $\Delta I = -1$ transition with the detectors at 0° and 100°. Figure 3 shows the same plot for a typical $\Delta I = 0$ transition.

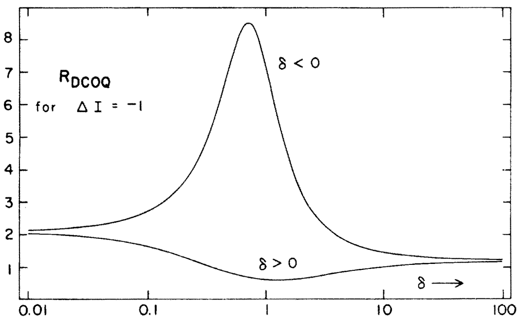

FIG. 2. Directional correlation from an orientated nucleus for a typical $\Delta I = -1$ transition with the detectors located at 0° and 100° with respect to the beam axis.

It is possible to draw several general guidelines for a quick interpretation of DCOQ ratios: (1) $R_{\mathrm{DCOQ}} = 1$ is characteristic (although not uniquely) of a $\Delta I = -2$, quadrupole transition, (2) $R_{\mathrm{DCOQ}} \simeq 2$ usually implies a $\Delta I = \pm 1$, pure-dipole transition, (3) $R_{\mathrm{DCOQ}} \gtrsim 3$ is uniquely characteristic of $\Delta I = \pm 1$ with a $\pm$ mixing ratio, and (4) $R_{\mathrm{DCOQ}} < 1$ implies $\Delta I = 0$ or $\Delta I = \pm 1$ with a mixing ratio near ∓ 1.

As noted above, the information that one gets from DCOQ is essentially the same as that determined from a singles anisotropy measurement. Since many γ-ray pairs are used in DCOQ, the uncertainty can easily be comparable to that obtained from angular distribution measurements. If the coincidence data is taken at only one pair of angles, no information is obtained which is comparable to the A_{44} in an angular distribution, consequently there can be more ambiguity in a DCOQ measurement than there is in an angular distribution.

C. Determination of γ-ray energies

Energy calibrations were done in beam, to correct for rate dependent effects, using five γ rays of known energy: three from Coulomb excitation

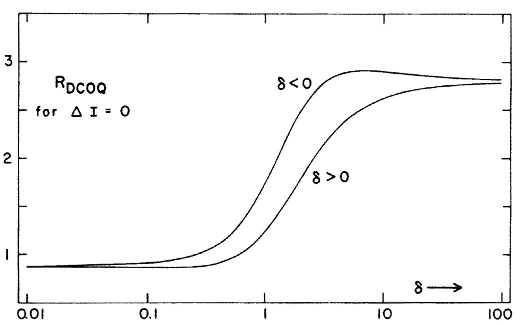

FIG. 3. Directional correlation from an orientated nucleus for a typical $\Delta I = 0$ transition with the detectors located at 0° and 100° with respect to the beam axis.

of the Au backing (191.48, 278.92, and 547.55 keV), and two from a ^{60}Co source placed near the detector. These energies were in turn measured relative to a source containing ^{182}Ta and ^{152}Eu. The energies of the Ta-Eu lines have been measured quite precisely.[19-21] The nonlinearity of the detector-amplifier-ADC (analog-to-digital converter) system was measured with the Ta-Eu source

TABLE I. Intensity analysis for γ rays emitted following the $^{94}Zr(^{13}C, 3n\gamma)^{104}Pd$ reaction at 47 MeV.

Energy (keV)	Relative intensity Singles	Coincidence	Adopted	Unresolved contaminants Energy (keV)	Origin	Intensity
116.3(2)	4.2(1)	1.6(6)	1.6(6)			
163.40(15)	4.4(1)	4.2(3)	4.4(1)			
193.37(20	1.9(1)	1.4(4)	1.9(1)			
201.08(20)	1.4(1)	1.1(3)	1.4(1)			
215.6(3)	6.7(1)	2.2(6)	2.2(6)	216	^{104}Rh	1.1
216.3(3)		3.0(4)	3.0(4)			
233.2(3)	2.8(1)	1.2(3)	1.2(3)			
250.97(5)	14.2(3)	14.3(5)	14.2(3)			
309.7(3)	3.2(1)	1.1(3)	1.1(3)	310.6	^{103}Pd	1.6
320.7(3)	2.5(1)	1.0(2)	1.0(2)			
350.0(2)	2.8(1)	1.9(3)	1.9(3)			
379.70(5)	22.6(5)	20.8(7)	20.8(7)			
401.44(15)	1.4(1)	1.3(3)	1.4(1)			
409.0(2)	8.0(2)	0.5(2)	0.5(2)			
409.46(10)		7.5(5)	7.5(5)			
467.5(2)	2.3(1)	1.6(3)	1.6(3)	467	^{104}Rh	0.8
497.05(10)	2.9(1)	2.5(4)	2.9(1)			
555.79(5)	100		100			
601.3(2)	3.2(2)	3.7(8)	3.2(2)			
602.8(2)	3.5(2)	4.2(8)	3.5(2)			
611.89(5)	15.8(3)	15.5(8)	15.8(3)			
617.73(5)	11.8(3)	11.9(7)	11.8(3)			
651.04(15)	3.1(1)	3.5(6)	3.1(1)			
679.76(5)	18.9(4)	19.5(9)	18.9(4)			
700.6(2)	2.8(1)	1.4(3)	1.4(3)			
738.61(5)	27.5(6)	27.7(9)	27.5(6)			
740.7(3)		1.7(8)	1.7(8)			
758.83(20)	1.4(1)	1.0(4)	1.4(1)			
767.80(5)	90.6(18)	90.9(24)	90.6(18)			
785.92(20)	1.9(1)	1.8(9)	1.9(1)			
797.04(10)	13.4(4)	11.8(7)	11.8(7)			
802.46(5)	18.8(5)	18.9(7)	18.8(5)			
858.08(15)	1.6(1)	1.5(6)	1.6(1)			
879.01(15)	6.8(2)	6.1(5)	6.8(2)			
915.25(10)	10.3(3)	10.1(6)	10.3(3)			
926.2(4)	68.7(14)	5.4(5)	5.4(5)			
926.21(10)		63.2(12)	63.2(12)			
941.3(2)	3.6(2)	2.7(9)	2.7(9)	941.2	^{103}Pd	2.1
970.88(10)	26.4(6)	23.2(10)	23.2(10)	970.1	^{103}Pd	6.7
974.38(20)	2.3(3)	3.8(8)	2.3(3)			
1032.70(15)	2.4(1)	2.4(4)	2.4(1)			
1058.71(15)	4.8(2)	4.7(4)	4.8(2)			
1064.15(20)	2.1(1)	2.1(3)	2.1(1)			
1167.79(5)	14.5(4)	13.9(9)	14.4(4)			
1172.04(20)	4.2(2)	4.4(6)	4.2(2)			
1265.08(20)	2.5(2)	2.2(9)	2.5(2)			
1341.7(2)	1.7(1)		1.7(1)			
1344.1(2)	2.9(2)	2.9(7)	2.9(2)			
1526.5(2)	1.7(1)	4.2(18)	1.7(1)			
1625.8(4)	2.1(2)	0.8(5)	0.8(5)			

so that the centroids of peaks in the data could be corrected. The final energy calibration was then determined from a linear least-squares fit to the five calibration lines in the corrected linear data. We believe the precision of this measurement to be ± 50 eV for uncontaminated lines between ~ 200 keV and ~ 1400 keV.

D. Linear polarization data

Linear polarization measurements were made in collaboration with Lee, Stromswold, and Elliott of Johns Hopkins University using a two-crystal Compton polarimeter. This experiment and the results have been described in a recent publication.[22] The polarization measurements are used to recognize parity-changing transitions and to remove ambiguities in spin assignments. For example, a $\Delta I = 0$ mixed transition can have an angular distribution which is indistinguishable from an $E2$ transition, but fortunately they have very different linear polarizations.

III. RESULTS FOR ^{104}Pd

A. γ-γ coincidence measurements

Relative intensities of γ transitions can be determined from the coincidence data by measuring the number of coincidence events between the γ ray of interest and a γ ray lower in the decay scheme. If more than one decay path is observed the intensities from each path must be summed. This coincidence intensity is proportional to the singles intensity for uncontaminated γ transitions. The proportionality constant was determined for the ^{104}Pd data from several intense, uncontaminat-

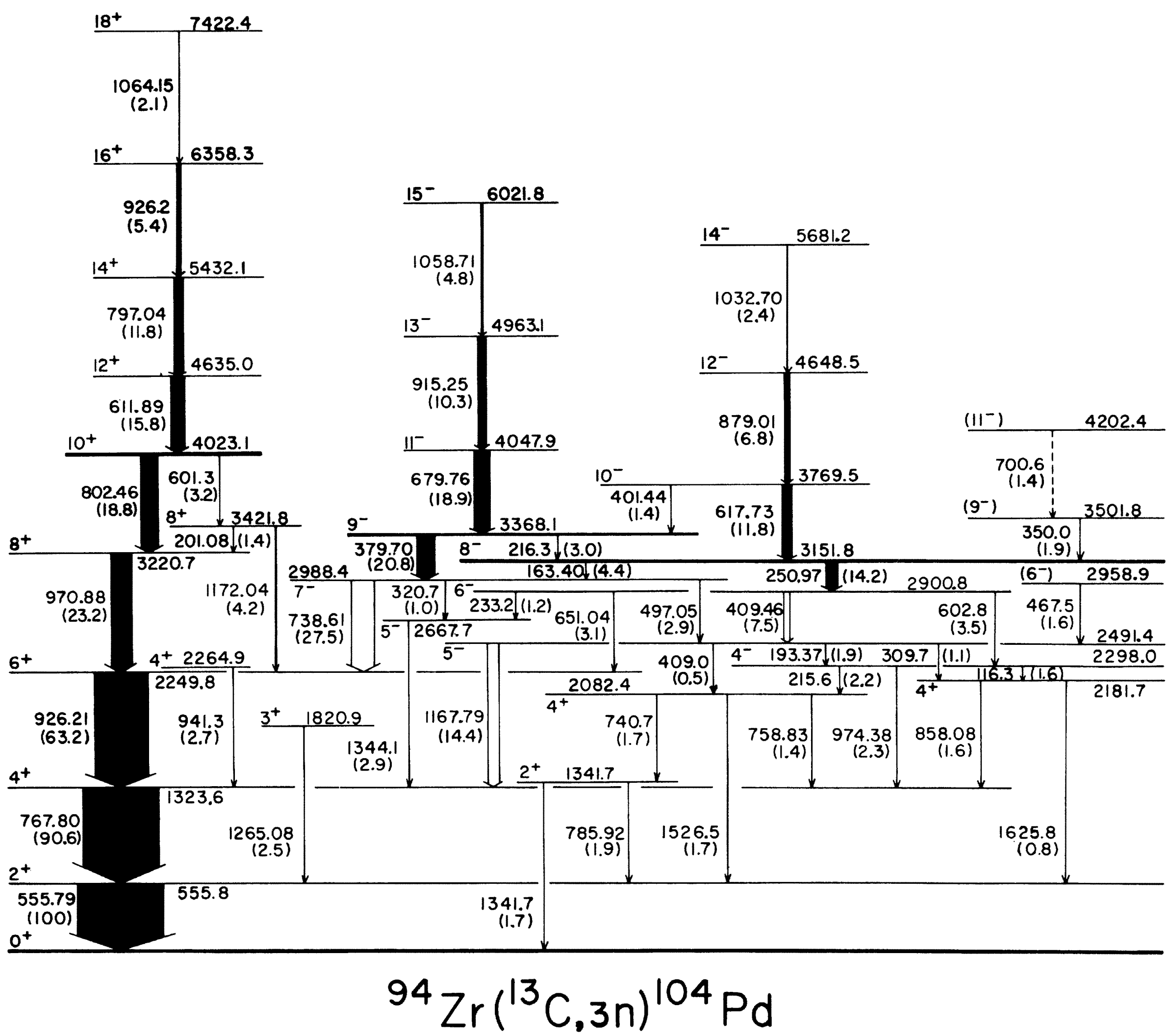

FIG. 4. Decay scheme for ^{104}Pd. Solid arrows indicate $E2$ transitions. Relative intensities are given in parentheses.

ed γ rays and was then used to calculate the coincidence intensities listed in column three of Table I. The second column contains the relative intensities of γ rays from the reaction $^{94}Zr(^{13}C, 3n)^{104}Pd$ at 47 MeV as determined from the A_0 coefficients of the singles angular distribution.

There are two reasons for possible disagreement between the singles and coincidence intensities: (1) the level scheme, upon which the coincidence calculation depends, may be incorrect, or (2) the γ rays may be contaminated by other lines in the singles spectra. Consequently, a list of known contaminants has been included in the last three columns of Table I. Intensities for these

TABLE II. Angular distribution analysis for γ rays assigned to ^{104}Pd.

Energy (keV)	$I_i^\pi \to I_f^\pi$	A_{22}	A_{44}	α_2	α_4	Mixing ratio
116 [a]	$4^- \to 4^+$	0.020(24)	0.032(30)	0.59(5)	0.24(10)	0.50(5) [a]
163	$8^- \to 7^-$	−0.794(27)	0.071(29)	0.70(4)	0.42(10)	−0.58(20) or −1.3(3)
193	$5^- \to 4^-$	0.33(3)	−0.02(4)	0.63(5)	0.29(10)	0.44(5)
201	$8^+ \to 8^+$	0.27(4)	0.00(5)	0.64(7)	0.46(10)	−0.15(15)
216 [b]	$9^- \to 8^-$	0.03(7)	0.073(28)	0.78(3)	0.48(8)	0.17(5) or >10
233 [a]	$6^- \to 5^-$	−0.24(3)	0.06(4)	0.66(4)	0.34(10)	−0.02(3) [a]
251	$8^- \to 6^-$	0.300(16)	−0.083(19)	0.70(4)	0.42(10)	
321 [a]	$7^- \to 5^-$	0.09(3)	−0.04(4)	0.20(7)	0.18(19)	
350 [a]	$9^- \to 8^-$	0.12(3)	0.03(4)	0.78(10)	0.48(15)	0.22(3) [a]
380	$9^- \to 7^-$	0.328(12)	−0.089(14)	0.78(3)	0.48(8)	
401	$10^- \to 9^-$	−0.85(7)	0.19(9)	0.71(4)	0.41(11)	−1.0(5)
409	$6^- \to 5^-$	0.498(16)	0.135(20)	0.66(4)	0.34(10)	0.70(8) or 1.9(3)
467 [a]	$6^- \to 5^-$	0.16(5)	0.04(6)	0.66(6)	0.34(15)	0.28(5) [a]
497	$7^- \to 5^-$	0.17(3)	−0.07(5)	0.39(8)	0.31(22)	
556	$2^+ \to 0^+$	0.272(7)	−0.066(7)	0.38(1)	0.04(1)	
601 [c]	$10^+ \to 8^+$	0.06(4)	−0.09(5)	0.14(9)	0.52(29)	
603 [c]	$6^- \to 4^-$	0.16(9)	0.12(13)	0.35(20)	−0.49(54)	
612	$12^+ \to 10^+$	0.260(11)	−0.099(15)	0.64(3)	0.61(9)	
618	$10^- \to 8^-$	0.296(15)	−0.071(20)	0.71(4)	0.41(11)	
651	$6^- \to 6^+$	0.26(4)	0.11(5)	0.66(4)	0.34(10)	−0.18(8)
680	$11^- \to 9^-$	0.314(15)	−0.086(19)	0.77(4)	0.51(11)	
701	$11^- \to 9^-$	0.25(7)	0.00(10)	0.62(17)	<0.59	
739	$7^- \to 6^+$	−0.294(11)	0.028(12)	0.75(3)	0.41(8)	−0.04(2)
759	$4^+ \to 4^+$	−0.11(8)	0.13(11)	0.55(10)	0.21(12)	−0.84(24)
768	$4^+ \to 2^+$	0.282(8)	−0.078(8)	0.55(2)	0.21(2)	
786	$2^+ \to 2^+$	−0.28(8)	0.18(12)	0.46(17)	0.06(4)	−4.8(42)
797	$14^+ \to 12^+$	0.285(14)	−0.114(18)	0.72(4)	0.75(12)	
802	$10^+ \to 8^+$	0.330(12)	−0.096(15)	0.80(3)	0.55(9)	
858	$4^+ \to 4^+$	0.47(13)	0.08(17)	0.55(10)	0.21(12)	0.45(30)
879	$12^- \to 10^-$	0.28(4)	−0.03(5)	0.70(10)	0.20(32)	
915 [d]	$13^- \to 11^-$	0.230(18)	−0.062(24)	0.57(5)	0.39(15)	
926 [a]	$6^+ \to 4^+$	0.290(8)	−0.087(9)	0.64(2)	0.36(4)	
941 [a]	$4^+ \to 4^+$	−0.04(5)	−0.02(7)	0.55(10)	0.21(12)	−0.64(14) or 5.0(23) [a]
971 [a]	$8^+ \to 6^+$	0.245(13)	−0.091(17)	0.57(3)	0.46(9)	
974	$4^- \to 4^+$	0.40(13)	−0.26(17)	0.59(5)	0.24(10)	0.5(6)
1033	$14^- \to 12^-$	0.31(6)	−0.19(8)	0.79(14)	1.22(51)	
1059 [d]	$15^- \to 13^-$	0.08(4)	−0.09(6)	0.21(10)	0.58(38)	
1064	$18^+ \to 16^+$	0.30(5)	−0.19(7)	0.77(12)	1.38(46)	
1168	$5^- \to 4^+$	−0.216(16)	−0.002(21)	0.63(5)	0.29(10)	0.00(2)
1265	$3^+ \to 2^+$	0.05(7)	0.02(9)	0.54(17)	0.14(14)	0.23(7) or $\lvert\delta\rvert > 13$
1342	$2^+ \to 0^+$	0.33(12)	0.11(17)	0.46(17)	<0.07	
1344	$5^- \to 4^+$	−0.31(6)	0.03(8)	0.67(4)	0.33(10)	−0.06(5)
1526	$4^+ \to 2^+$	0.24(9)	−0.24(13)	0.48(18)	0.66(35)	
1626	$4^+ \to 2^+$	0.22(15)	−0.09(20)	0.44(29)	0.25(55)	

[a] No correction has been made for γ-ray contamination in the singles spectra.

[b] Corrected for the presence of 33% $E1$ ($4^- \to 4^+$). Uncorrected values are $A_{22} = 0.144(12)$ and $A_{44} = 0.042(15)$.

[c] Interference from (n, n') on ^{74}Ge.

[d] Possibly Doppler broadened.

contaminant lines were extracted from the coincidence data. In most cases where the singles and coincidence intensities did not agree, the source of contamination could be determined. The fourth column of Table I lists the adopted relative intensities for the γ transitions in ^{104}Pd. These intensities were usually taken as the singles intensities when the two numbers agreed or the coincidence intensity if they disagreed.

The level scheme proposed for ^{104}Pd is shown in Fig. 4. The adopted relative intensities for all transitions are given in parentheses below or to the right of the γ-ray energies and are also indicated roughly by the width of the arrows in the figure. Solid arrows indicate $E2$ transitions. In order to place a γ ray in this level scheme we insist not only that all of the implied coincidence relations exist but also that the quantitative coincidence intensities be consistent with the placement. The latter requirement implies that (i) the coincidence and singles intensities be equal for uncontaminated transitions and (ii) that all coincidences with transitions lower in the cascade have equal intensity.

The placement of a second 926-keV transition at 6358 keV in addition to the more intense 926-keV transition at 2250 keV illustrates the importance of these requirements. There are three aspects of the coincidence data which support this placement: (1) the 926-keV γ ray is in coincidence with itself with a corrected (half the observed) coincidence intensity of 6.1 ± 0.7 units, (2) all four transitions between the 14^+ and 6^+ are more strongly in coincidence with the 926 than with any other transition below them by an average amount of 4.4 ± 0.9 units, and (3) the 1064-926 coincidence is about twice as strong as any other coincidence with the 1064, and indeed twice as strong as the 1064 singles intensity would predict. The final two observations appear to contradict intensity requirement (ii), and together with the first observation can be explained only by the placement of a 16^+ to 14^+ 926-keV transition with 5.4 ± 0.5 units of intensity. This example illustrates the advantage of a quantitative coincidence analysis, since without accurate intensities the only information available would be an observed 926-926 coincidence, and no placement could have been made.

B. Angular momentum analysis

The angular distributions were fitted according to

$$W(\theta) = A_0 Q_0 \left[1 + A_{22}\frac{Q_2}{Q_0}P_2(\cos\theta) + A_{44}\frac{Q_4}{Q_0}P_4(\cos\theta)\right],$$

where the Q_k are solid-angle correction factors, A_0 is a measure of the total γ-ray intensity, and the A_{kk} determine the multipolarity of the transition. The angular-distribution coefficients A_{kk} are related to those for maximum alignment A^0_{kk} by the attenuation coefficients α_k:

$$A_{kk} = \alpha_k A^0_{kk}.$$

The mixing ratios listed in Table II are defined

TABLE III. Average DCOQ ratios from the coincidence data for most of the transitions assigned to ^{104}Pd. Detector angles were 90° and −30°.

Energy (keV)	$I_i^\pi \to I_f^\pi$	$R_{\rm DCOQ}$
	$\Delta I = -1$ transitions with $\delta \simeq -1$	
163.40	$8^- \to 7^-$	4.7(7)
401.44	$10^- \to 9^-$	9(6)
	$\Delta I = -1$ transitions with $\delta \simeq +1$	
193.37	$5^- \to 4^-$	1.2(5)
216.3 [a]	$9^- \to 8^-$	0.73(31)
350.0 [a]	$9^- \to 8^-$	0.71(26)
409.46	$6^- \to 5^-$	0.83(7)
	$\Delta I = -1$ transitions with $\delta \simeq 0$	
233.2 [a]	$6^- \to 5^-$	1.9(8)
738.61	$7^- \to 6^+$	1.87(11)
1167.79	$5^- \to 4^+$	1.82(18)
1344.1	$5^- \to 4^+$	2.2(11)
	$\Delta I = -2$, $E2$ transitions	
250.97	$8^- \to 6^-$	0.93(6)
320.7 [a]	$7^- \to 5^-$	1.20(27)
379.70	$9^- \to 7^-$	1.02(6)
497.05	$7^- \to 5^-$	1.26(28)
555.79	$2^+ \to 0^+$	0.99(4)
611.89	$11^- \to 9^-$	0.93(6)
617.73	$10^- \to 8^-$	1.00(8)
679.76	$11^- \to 9^-$	0.95(6)
767.80	$4^+ \to 2^+$	1.07(5)
797.04	$14^+ \to 12^+$	0.86(7)
802.46	$10^+ \to 8^+$	0.94(6)
879.01	$12^- \to 10^-$	1.01(14)
915.25	$13^- \to 11^-$	1.16(12)
926.21 [a]	$6^+ \to 4^+$	1.08(5)
970.88 [a]	$8^+ \to 6^+$	0.91(6)
1032.70	$14^- \to 12^-$	0.95(27)
1058.71	$15^- \to 13^-$	1.21(20)
1064.15	$18^+ \to 16^+$	1.15(32)
1172.04	$8^+ \to 6^+$	1.00(28)
	Remaining transitions	
215.6 [a]	$4^- \to 4^+$	0.94(21)
467.5 [a]	$6^- \to 5^-$	1.03(28)
651.04	$6^- \to 6^+$	0.96(15)
758.83	$4^+ \to 4^+$	4.7(29)
941.3 [a]	$4^+ \to 4^+$	0.85(24)
974.38	$4^- \to 4^+$	0.9(4)
1265.08	$3^+ \to 2^+$	1.6(14)

[a] Transition is contaminated in the singles spectra.

as

$$\delta \equiv \langle \| E2 \| \rangle / \langle \| M1 \| \rangle \text{ or } \langle \| M2 \| \rangle / \langle \| E1 \| \rangle$$

with the sign convention of Krane and Steffen.[23] The attenuation coefficients α_1 and α_2 for all mixed transitions were determined from those of neighboring $E2$ transitions taking into account any necessary deorientation due to γ-ray emission. With the exception of the 1059-keV γ ray all of the transitions in the $\Delta I = -2$ cascades display coefficients characteristic of $E2$ transitions ($A_{22} \simeq 0.3$ and $A_{44} \simeq -0.1$). The A_{22} coefficient of the 1059-keV transition has been reduced by Doppler broadening of the line shape.

Since few γ rays in ^{104}Pd have significant interference, the DCOQ results in Table III are presented as a consistency check for the angular momentum assignments and for the decay scheme. It was not necessary to determine mixing ratios from DCOQ, so we took less coincidence data for ^{104}Pd than ^{102,106}Pd. Transitions with similar multipolarities have been grouped together so the reader can see that the general characteristics given above for DCOQ are confirmed for ^{104}Pd.

C. Discussion of the ^{104}Pd level scheme

The combination of experiments described above permits us to have great confidence in the level scheme shown in Fig. 4. Since the 739-, 651-, and 1168-keV transitions all feed states in the ground-state band and the linear polarization measurements[22] show that they change parity, the corresponding 7^-, 6^-, and 5^- states must have negative parity. In addition, the large $E2/M1$ mixing ratio observed for the 409-keV transition confirms that the 6^- and 5^- states have the same parity. The large $E2/M1$ mixing ratios observed for the 216- and 163-keV transitions and the $E2$ character of the 380- and 251-keV transitions show that the 9^-, 8^-, and 7^- states have the same parity. The negative parity of the higher-energy states is confirmed by the $E2$ character of the connecting transitions. (The $E2$ transitions are uniquely established by combining angular distributions and linear polarization measurements.)

IV. RESULTS FOR ^{106}Pd

A. γ-γ coincidence measurements

Table IV lists precise energies and relative intensities for all γ transitions assigned to ^{106}Pd from the ^{96}Zr(^{13}C, $3n\gamma$)^{106}Pd reaction at 45 MeV. Because of impurities in the ^{96}Zr target (7% ^{90}Zr, 2% ^{92}Zr, and 4% ^{94}Zr), the spectrum is very complex and the coincidence data are especially valuable in unraveling the level scheme. There are obviously many γ rays here whose singles angular distributions may be erroneous.

The level scheme for ^{106}Pd is shown in Fig. 5. It was difficult to normalize relative intensities to the 511.8-keV ground-state transition because of the 511-keV annihilation radiation which is present. The 511.8 intensity was obtained by summing the intensities of all observed transitions feeding the 511.8-keV state and estimating the unobserved feeding (2%) by comparison to ^{102,104}Pd. A second problem is the impurity of the 717.3-keV, $4^+ \to 2^+$ transitions. The 717-512 coincidence intensity turns out to be a measure of the intensity of both the 717.3- and the 717.1-keV, $7^- \to 6^+$ transition. The intensity of the 717.1 was determined from two sources: (1) the 717-717 coincidence intensity, and (2) the difference between the 847-717 and the 847-512 coincidence intensities. The 717.1 intensity was then subtracted from the total 717-keV intensity coming from ^{106}Pd to determine the intensity of the 717.3-keV transition.

Most of the 511-keV annihilation quanta were produced by pair production when high-energy γ rays struck the lead absorber which was inside the chamber to reduce Compton scattering from one detector to the other. Thus the coincidence data involving the 512-keV, $2^+ \to 0^+$ transition were contaminated since these 511-keV quanta were in true coincidence with every prompt transition in ^{106}Pd. The extra intensity in the 512-keV coincidence gate was determined by comparing the number of coincidences among strong γ rays to the 512-keV coincidence events with those same γ rays. Once this correction (20%) was determined, the coincidence rates for weak lines coincident with the 512-keV γ ray could be used in the analysis.

B. Angular momentum analysis

The distribution coefficients for two γ rays given in Table V have been corrected for the presence of known contamination. The 717.3-keV, $4^+ \to 2^+$ transition is completely unresolvable from the 717.1-keV, $7^- \to 6^+$ transition which accounts for 11% of the total strength. The 717.1 was assumed to be pure $E1$ in making the correction. The 901.1-keV, $7^- \to 6^+$ transition was unresolvable from a 901.7-keV, $8^+ \to 6^+$ transition in ^{102}Pd which accounts for 46% of the total strength. The coefficients for the 901.7-keV γ ray could be inferred from those of neighboring transitions in ^{102}Pd. These coefficients were then appropriately subtracted from the summed coefficients to determine the quoted coefficients for the 901.1-keV γ ray.

Average DCOQ ratios from the coincidence data

TABLE IV. Intensity analysis for γ rays emitted following the $^{96}Zr(^{13}C, 3n\gamma)^{106}Pd$ reaction at 45 MeV.

Energy (keV)	Relative intensity: Singles	Relative intensity: Coincidence	Relative intensity: Adopted	Unresolved contaminants: Energy (keV)	Unresolved contaminants: Origin	Unresolved contaminants: Intensity
199.0(3)	1.8(2)	1.2(2)	1.2(2)			
205.11(5)	8.7(3)	8.9(4)	8.8(3)			
221.40(20)	0.8(2)	1.0(2)	0.9(2)			
285.0(5)	0.7(2)	0.6(2)	0.6(2)			
290.89(10)	3.8(2)	3.6(1)	3.6(1)			
299.39(10)	8.6(3)	8.6(4)	8.6(3)			
301.99(10)	10.7(3)	10.3(3)	10.3(3)			
367.6(2)	1.1(2)	0.4(1)	0.4(1)			
383.11(20)	3.2(2)	2.6(3)	2.6(3)			
384.9(3)	0.7(2)	0.4(2)	0.4(2)			
393.36(20)	1.4(2)	1.5(3)	1.4(2)			
396.26(5)	14.0(4)	13.9(5)	13.9(3)			
412.8(3)	1.7(2)	0.8(2)	0.8(2)			
429.8(3)	3.2(3)	2.6(2)	2.6(2)			
463.03(20)	1.5(3)	1.3(2)	1.4(2)			
477.0(3)	3.6(2)	1.6(3)	1.6(3)	476.7	^{103}Pd	1.6
484.2(3)	1.4(3)	0.9(2)	0.9(2)			
495.97(5)	5.7(3)	5.7(4)	5.7(3)			
511.78(10)	137		100 [a]	511.0	Annihilation	37
				555.6	^{101}Pd	0.6
555.2(2)	32.6(8)	20.0(5)	20.0(5)	555.8	^{104}Pd	7.6
				556.4	^{102}Pd	4.4
570.47(5)	30.5(8)	27.1(7)	27.1(7)			
616.22(15)	2.9(4)	3.1(4)	3.0(3)			
633.1(3)	3.8(2)	1.2(3)	1.2(3)	631.9	^{102}Ru	2.7
655.40(15)	7.4(4)	5.9(4)	5.9(4)			
668.1(3)	5.4(3)	2.2(3)	2.2(3)	667.2	^{101}Pd	2.8
682.2(2)	2.0(3)	1.7(2)	1.7(2)			
697.96(20)	2.5(3)	3.0(3)	2.7(2)			
717.1(4)	95.8(21)	11.2(7)	11.2(7)	717.7	^{103}Pd	1.6
717.31(10)		88.5(20)	88.5(20)	719.3	^{102}Pd	3.6
732.07(10)	5.1(4)	5.3(3)	5.2(3)			
748.3(2)	4.8(3)	3.0(2)	3.0(2)			
797.9(3)	5.9(4)	2.7(4)	2.7(4)	798.6	^{100}Pd	3.6
804.3(4)	14.0(5)	2.0(4)	2.0(4)			
805.1(2)		9.1(3)	9.1(3)			
808.4(2)	5.9(4)	3.0(2)	3.0(2)	808.8	^{105}Pd	2.6
847.43(2)	62.1(14)	58.8(16)	58.8(16)	847.6	^{105}Pd	6.2
876.3(3)	3.7(3)	1.2(7)	1.2(7)	877.7	^{101}Pd	0.7
877.5(3)		1.5(5)	1.5(7)			
885.97(5)	37.8(9)	36.0(9)	36.0(9)			
901.1(2)	4.1(4)	2.2(4)	2.2(4)	901.7	^{102}Pd	1.9
968.4(3)	3.8(3)	2.5(2)	2.5(2)			
986.1(3) [b]	5.7(3)	2.0(5)	2.0(5)			
986.1(3) [c]		2.0(2)	2.0(2)			
1000.0(3)	5.4(3)	2.2(5)	2.2(5)	1000.9	^{105}Pd	1.0
1001.2(3)		2.1(2)	2.1(2)			
1017.9(4)	2.2(3)	1.3(2)	1.3(2)			
1045.94(10)	5.9(3)	6.0(5)	5.9(3)			
1127.93(20)	1.7(3)		1.7(3)			
1168.25(5)	26.0(7)	26.0(10)	26.0(6)			
1188.3(2)	1.2(2)	1.2(2)	1.2(2)			
1315.3(3)	1.4(3)	1.3(2)	1.3(2)			
1349.5(2)	1.6(3)	1.8(3)	1.7(2)			
1572.9(3)	1.0(3)	1.1(4)	1.0(3)			

[a] See text.
[b] $10^+ \to 8^+$.
[c] $12^- \to 10^-$.

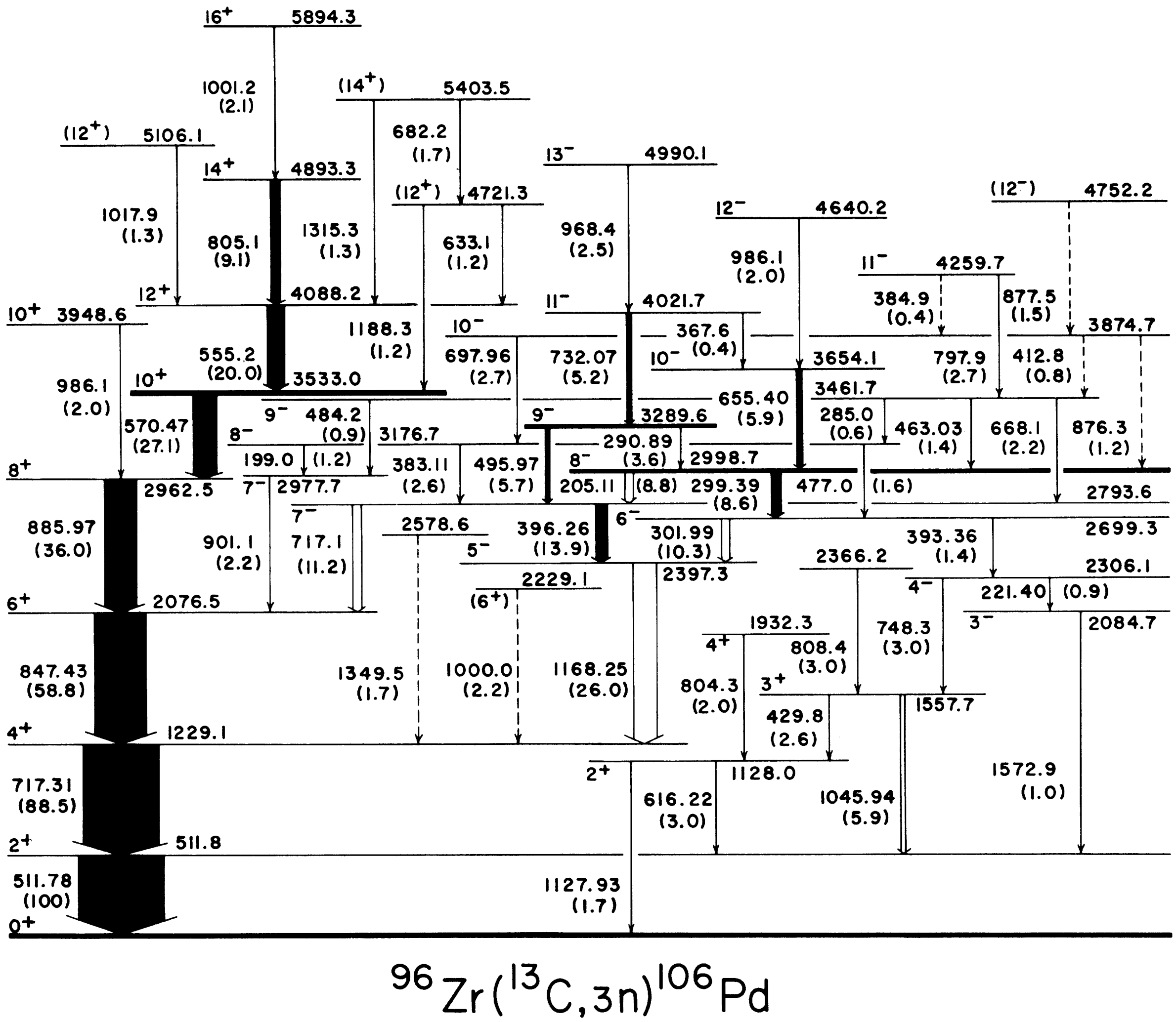

FIG. 5. Decay scheme for ^{106}Pd. Solid arrows indicate $E2$ transitions. Relative intensities are given in parentheses.

for most of the transitions assigned to ^{106}Pd are listed in Table VI. Since many γ rays in ^{106}Pd are contaminated in the singles spectra, we recorded extra coincidence data to obtain accurate DCOQ ratios. Five transitions display the characteristic $R_{\mathrm{DCOQ}} > 3$ of a $\Delta I = -1$ transition with $\delta \simeq -1$. Two of these transitions (199 and 413 keV) are weak and contaminated so that the singles angular distribution produced no useful information. The one $\Delta I = -1$ transition with $\delta \simeq 1$ yields $R_{\mathrm{DCOQ}} \lesssim 1$ as expected. Five additional $\Delta I = -1$ transitions have been assigned mixing ratios near zero. These all display the characteristic $R_{\mathrm{DCOQ}} \simeq 2$. The 748-keV γ ray, which was contaminated in the singles data, is consistent here with being pure $E1$ as suggested by Weight *et al.*[15]

Notice that the uncertainties obtained for δ from DCOQ are as good as those obtained from the angular distribution. However, in several cases there are two equally valid results from DCOQ. It is impossible to distinguish between these two solutions since DCOQ does not have information equivalent to the A_{44} in an angular distribution.

C. Discussion of the ^{106}Pd level scheme

Our angular distribution and linear polarization[22] measurements have definitely established that an $E1$ transition (1168 keV) connects the 5^- state at 2397.3 keV to the 4^+ member of the ground-state band. The angular distribution of the 6^- to 5^- transition is unusual, clearly indicating a highly mixed, $\Delta I = 1$ transition and thus no change of parity. The angular distribution and linear polarization measurements also show that the 13^- (968 keV) 11^- (732 keV) 9^- (496 keV) 7^- (396 keV) 5^-

cascade and the 12^- (986 keV) 10^- (655 keV) 8^- (299 keV) 6^- cascade are composed of $E2$ transitions. Many other states which were connected to these states by mixed $E2/M1$ transitions definitely can be assigned negative parity. The 6^+ state we observe at 2076.5 keV is not the same as the 2077.4-keV, 3^+ or 4^+ state observed in decay experiments[16]; the difference in energy is much larger than the combined uncertainty in the two measurements.

V. RESULTS FOR ^{102}Pd

A. γ-γ coincidence measurements

The intensity analysis for γ rays emitted following the $^{92}Zr(^{13}C, 3n\gamma)^{102}Pd$ reaction at 51 MeV is given in Table VII, while Fig. 6 shows the proposed level scheme. Due to an unusually large amount of contamination caused by γ-ray energy overlap, it has been necessary to rely heavily on the γ-γ

TABLE V. Angular distribution analysis for γ rays assigned to ^{106}Pd.

Energy (keV)	$I_i^\pi \to I_f^\pi$	A_{22}	A_{44}	α_2	α_4	Mixing ratio
205	$8^- \to 7^-$	0.103(9)	0.028(12)	0.81(3)	0.42(8)	0.21(2)
221	$4^- \to 3^-$	−0.18(10)	−0.01(11)	0.63(15)	0.26(12)	0.03(8) or −9(5)
285	$9^- \to 8^-$	−1.08(12)	0.17(18)	0.86(10)	0.75(25)	−0.9(5)
291	$9^- \to 8^-$	0.253(28)	0.01(4)	0.67(8)	0.72(24)	0.36(4)
299	$8^- \to 6^-$	0.348(13)	−0.083(15)	0.81(3)	0.42(8)	
302	$6^- \to 5^-$	0.504(18)	0.044(23)	0.71(12)	0.34(10)	0.64(22)
383	$8^- \to 7^-$	−0.89(4)	0.01(5)	0.81(6)	0.42(16)	−0.55(25)
393	$6^- \to 4^-$	0.32(6)	0.01(10)	0.71(12)	<0.39	
396	$7^- \to 5^-$	0.273(11)	−0.088(14)	0.62(3)	0.41(6)	
430	$3^+ \to 2^+$	0.02(4)	0.01(5)	0.49(15)	0.12(11)	0.20(4) or < −12
463	$9^- \to 8^-$	−1.27(12)	0.22(14)	0.86(10)	0.75(25)	−0.9(5)
496	$9^- \to 7^-$	0.28(3)	−0.13(4)	0.76(8)	0.72(24)	
512 [a]	$2^+ \to 0^+$	0.201(9)	−0.060(11)	0.28(1)	0.035(6)	
555 [a]	$12^+ \to 10^+$	0.277(10)	−0.089(11)	0.69(3)	0.55(7)	
570	$10^+ \to 8^+$	0.300(10)	−0.093(11)	0.72(2)	0.53(6)	
616	$2^+ \to 2^+$	−0.07(3)	−0.04(4)	0.24(11)	0.01(3)	<−4 or >25
655 [a]	$10^- \to 8^-$	0.227(30)	−0.06(4)	0.55(7)	0.31(24)	
717 [b]	$4^+ \to 2^+$	0.243(10)	−0.069(10)	0.48(2)	0.19(3)	
732	$11^- \to 9^-$	0.30(5)	−0.16(7)	0.72(13)	0.93(42)	
748 [a]	$4^- \to 3^+$	0.10(5)	0.06(6)	0.63(15)	0.30(15)	0.24(4) [a]
805 [a]	$14^+ \to 12^+$	0.205(16)	−0.068(22)	0.52(4)	0.45(14)	
808 [a]		0.23(5)	−0.04(5)	0.49(9)	0.15(17)	
847 [a]	$6^+ \to 4^+$	0.264(9)	−0.075(9)	0.58(2)	0.31(4)	
877 [a]	$\{12^- \to 10^-$, $10^- \to 8^-\}$	0.25(4)	−0.12(5)	0.62(11)	0.73(32)	
886	$8^+ \to 6^+$	0.275(11)	−0.092(12)	0.64(3)	0.46(6)	
901 [c]	$7^- \to 6^+$	−0.33(10)	0.02(9)	0.78(6)	0.52(12)	−0.06(7)
968 [a]	$13^- \to 11^-$	0.27(11)	−0.14(14)	0.67(27)	0.87(87)	
986 [a]	$\{12^- \to 10^-$, $10^+ \to 8^+\}$	0.25(12)	−0.10(14)	0.61(29)	0.61(82)	
1001 [a]	$\{16^+ \to 14^+$, $6^+ \to 4^+\}$	0.15(4)	−0.03(5)			
1018 [a]	$12^+ \to 12^+$	0.22(10)	−0.01(14)	0.69(5)	0.55(10)	−0.36(30) [a]
1046	$3^+ \to 2^+$	−0.19(4)	0.06(5)	0.49(15)	0.12(11)	0.01(7) or −4.5(13)
1128	$2^+ \to 0^+$	0.17(8)	0.08(11)	0.24(11)	−0.05(6)	
1168	$5^- \to 4^+$	−0.256(10)	0.022(10)	0.60(6)	0.30(10)	−0.04(2)
1349		0.07(9)	−0.09(12)	0.58(15)	0.31(15)	
1573	$3^- \to 2^+$	−0.44(16)	0.20(21)	0.56(15)	0.16(15)	−0.19(18)

[a] Uncorrected for contamination in singles spectra.
[b] Corrected for the presence of 11% $E1$ ($7^- \to 6^+$). Uncorrected values $A_{22} = 0.200(7)$, $A_{44} = -0.062(7)$.
[c] Corrected for the presence of 46% $E2$ (901.7 keV from ^{102}Pd. Uncorrected values $A_{22} = 0.14(4)$ $A_{44} = 0.00(6)$.

TABLE VI. Average DCOQ ratios from the coincidence data for most of the transitions assigned to ^{106}Pd. Detector angles were 100° and 0°.

Energy	$I_i^\pi \rightarrow I_f^\pi$	R_{DCOQ}	Mixing ratio From DCO	Mixing ratio From AD
		$\Delta I = -1$ transitions with $\delta \simeq -1$		
199.9 [a]	$8^- \rightarrow 7^-$	7.7(28)	−0.44(15) or −1.4(3)	
285.0	$9^- \rightarrow 8^-$	7(4)	−0.37(25) or −1.8(9)	−0.9(5)
383.11	$8^- \rightarrow 7^-$	6.5(16)	−0.38(11) or −1.5(3)	−0.55(25)
412.8 [a]	$10^- \rightarrow 9^-$	4.5(25)	−0.17(20) or −2.8(15)	
463.03	$9^- \rightarrow 8^-$	4.6(14)	−0.24(10) or −1.8(4)	−0.9(5)
		$\Delta I = -1$ transition with $\delta \simeq +1$		
301.99	$6^- \rightarrow 5^-$	0.77(6)	0.62(7)	0.64(22)
		$\Delta I = -1$ transitions with $\delta \simeq 0$		
748.3 [a]	$4^- \rightarrow 3^+$	1.4(4)	0.08(20)	0.24(4) [a]
901.1 [a]	$7^- \rightarrow 6^+$	1.7(4)	0.09(10)	−0.06(7) [a]
1045.94	$3^+ \rightarrow 2^+$	1.81(25)	−0.01(10) or −2.1(10)	0.01(7) or −4.5(13)
1168.25	$5^- \rightarrow 4^+$	2.06(11)	−0.05(3)	−0.04(2)
1572.9	$3^- \rightarrow 2^+$	3.0(19)	−0.3(7)	−0.19(18)
		$\Delta I = -2, E2$ transitions		
299.39	$8^- \rightarrow 6^-$	0.90(8)		
393.36	$6^- \rightarrow 4^-$	0.51(17)		
396.26	$7^- \rightarrow 5^-$	0.98(6)		
477.0 [a]	$8^- \rightarrow 6^-$	0.72(15)		
495.97	$9^- \rightarrow 7^-$	0.87(9)		
511.78 [a]	$2^+ \rightarrow 0^+$	1.05(5)		
555.2 [a]	$12^+ \rightarrow 10^+$	0.99(5)		
570.47	$10^+ \rightarrow 8^+$	0.97(4)		
655.40 [a]	$10^- \rightarrow 8^-$	1.17(12)		
668.1 [a]	$9^- \rightarrow 7^-$	0.82(19)		
682.2	$14^+ \rightarrow 12^+$	0.90(19)		
697.96	$10^- \rightarrow 8^-$	0.78(17)		
717.31 [a]	$4^+ \rightarrow 2^+$	1.05(4)		
732.07	$11^- \rightarrow 9^-$	0.87(10)		
797.9 [a]	$11^- \rightarrow 9^-$	0.89(21)		
804.3 [a]	$4^+ \rightarrow 2^+$	1.0(8)		
805.1 [a]	$14^+ \rightarrow 12^+$	1.05(7)		
808.4 [b]		0.70(16)		
847.43 [a]	$6^+ \rightarrow 4^+$	0.95(4)		
885.97	$8^+ \rightarrow 6^+$	0.98(4)		
968.4 [a]	$13^- \rightarrow 11^-$	1.11(19)		
986.1 [a]	$10^+ \rightarrow 8^+$	1.17(35)		
986.1 [a]	$12^- \rightarrow 10^-$	1.04(26)		
1001.2 [c]	$16^+ \rightarrow 14^+$	2.1(6)		
1188.3	$12^+ \rightarrow 10^+$	1.6(6)		
1315.3	$14^+ \rightarrow 12^+$	1.4(6)		
		Remaining transitions		
205.11	$8^- \rightarrow 7^-$	1.48(13)	0.14(5)	0.21(2)
221.40	$4^- \rightarrow 3^-$	1.4(5)	0.14(20) or < −2.5	0.03(8) or −9(5)
290.89	$9^- \rightarrow 8^-$	1.27(14)	0.21(7)	0.36(4)
429.8	$3^+ \rightarrow 2^+$	1.29(34)	0.18(17) or < −2.5	0.20(4) or < −12
616.22 [b]	$2^+ \rightarrow 2^+$	0.75(16)	0.8(7)	<−4 or >25
1017.9 [a]	$12^+ \rightarrow 12^+$	1.5(4)	−0.8(4)	−0.36(30)
1349.5		1.6(5)		

[a] Transition is contaminated in the singles spectra.
[b] These ratios involve only the 511.8 keV γ ray.
[c] Possibly Doppler broadened.

coincidence data to determine transition strengths and spin assignments in ^{102}Pd. In addition to the many strong contaminants listed in Table VII as coming from other nuclei, there are five cases (336, 714, 756, 979, and 1019 keV) in which both of the unresolved transitions belong to ^{102}Pd. Unresolved γ rays can be quite confusing; however, the coincidence analysis used in this experiment provides reliable placement for all but two γ rays: it is possible that the order of the 757-keV and 701-keV γ rays feeding the 7^- state should be reversed.

TABLE VII. Intensity analysis for γ rays emitted following the $^{92}Zr(^{13}C, 3n\gamma)^{102}Pd$ reaction at 51 MeV.

Energy (keV)	Relative intensity Singles	Coincidence	Adopted	Unresolved contaminants Energy	Origin	Intensity
156.7(2)	9.6(2)	1.1(5)	1.1(5)	156.6	^{102}Rh	8.7
173.26(15)	2.4(1)	2.3(5)	2.4(1)			
179.73(15)	5.9(1)	6.3(5)	5.9(1)			
182.83(15)	3.3(1)	3.1(3)	3.3(2)			
274.1(2)	4.7(1)	3.1(3)	3.1(3)			
327.20(5)	8.3(2)	6.9(3)	6.9(3)	327	^{101}Pd	0.7
336.0(2)	16.9(4)	5.6(4)	5.6(4)			
336.4(2)		8.5(6)	8.5(6)			
338.1(2)	2.6(2)	2.8(8)	2.6(2)			
387.50(10)	2.7(1)	3.2(3)	2.9(3)			
439.7(2)	13.2(3)	9.3(7)	9.3(7)	438	^{102}Rh	2.1
482.43(10)	2.5(1)	3.2(6)	2.5(1)			
508.3(3)	5.5(2)	3.6(5)	3.6(5)			
539.7(2)	7.5(2)	4.4(4)	4.4(4)	540.2	^{100}Ru	2.4
556.41(5)	109		100	555.7	^{101}Pd	9.0
590.0(3)	2.1(3)	2.0(5)	2.1(3)			
619.4(2)	4.0(1)	3.1(4)	3.1(4)	618.6	^{101}Pd	1.2
647.18(5)	8.0(2)	7.1(8)	7.9(2)			
701.22(10)	4.8(2)	5.8(6)	4.8(2)			
704.95(5)	20.5(5)	19.4(11)	20.3(5)			
713.8(2)	27.0(7)	12.2(11)	12.2(11)	714.0	^{103}Pd	2.1
714.7(2)		14.0(9)	14.0(9)			
719.34(10)	89.9(19)	81.6(22)	81.6(22)	719.8	^{99}Ru	12.4
756.5(2)	11.2(3)	7.4(9)	7.4(9)			
756.7(2)		3.5(8)	3.5(8)			
776.3(2)	10.4(3)	8.4(6)	8.4(6)	777.2	^{99}Ru	2.9
835.49(5)	60.9(13)	61.9(17)	61.3(10)			
890.7(3)	10.4(3)	4.0(11)	4.0(11)	891.1	^{101}Pd	3.2
893.14(7)	13.8(3)	13.3(8)	13.7(3)			
901.71(5)	49.7(11)	50.1(13)	49.8(8)			
931.9(2)	9.5(2)	5.4(7)	5.4(7)	931.6	^{99}Ru	3.1
962.2(2)	4.8(2)	3.2(6)	3.2(6)			
978.3(4)	24.4(5)		0.8(3) [a]			
979.66(5)		24.6(9)	24.4(5)			
988.45(20)	3.5(1)	3.2(6)	3.5(1)			
1003.3(2)	5.0(2)	3.5(6)	3.5(6)			
1018.6(3)	12.3(3)	5.2(7)	5.2(7)			
1019.0(3)		7.1(7)	7.1(7)			
1062.41(5)	10.4(3)	10.1(5)	10.3(3)			
1083.53(15)	4.4(2)	3.7(5)	4.3(2)			
1116.3(2)	4.2(1)	3.4(5)	4.0(4)			
1198.37(10)	3.4(1)	4.0(7)	3.4(1)			
1228.94(20)	1.4(1)	1.9(5)	1.4(1)			
1278.31(15)	3.6(1)	3.3(6)	3.6(1)			
1534.7(2)	0.9(1)		0.9(1)			
1555.16(20)	2.8(1)	3.9(9)	2.8(1)			
1581.29(20)	9.4(2)	8.9(10)	9.4(2)			
1744.5(3)	2.1(6)	2.1(13)	2.1(6)			

[a] Intensity calculated from branching ratios in decay studies (Ref. 11).

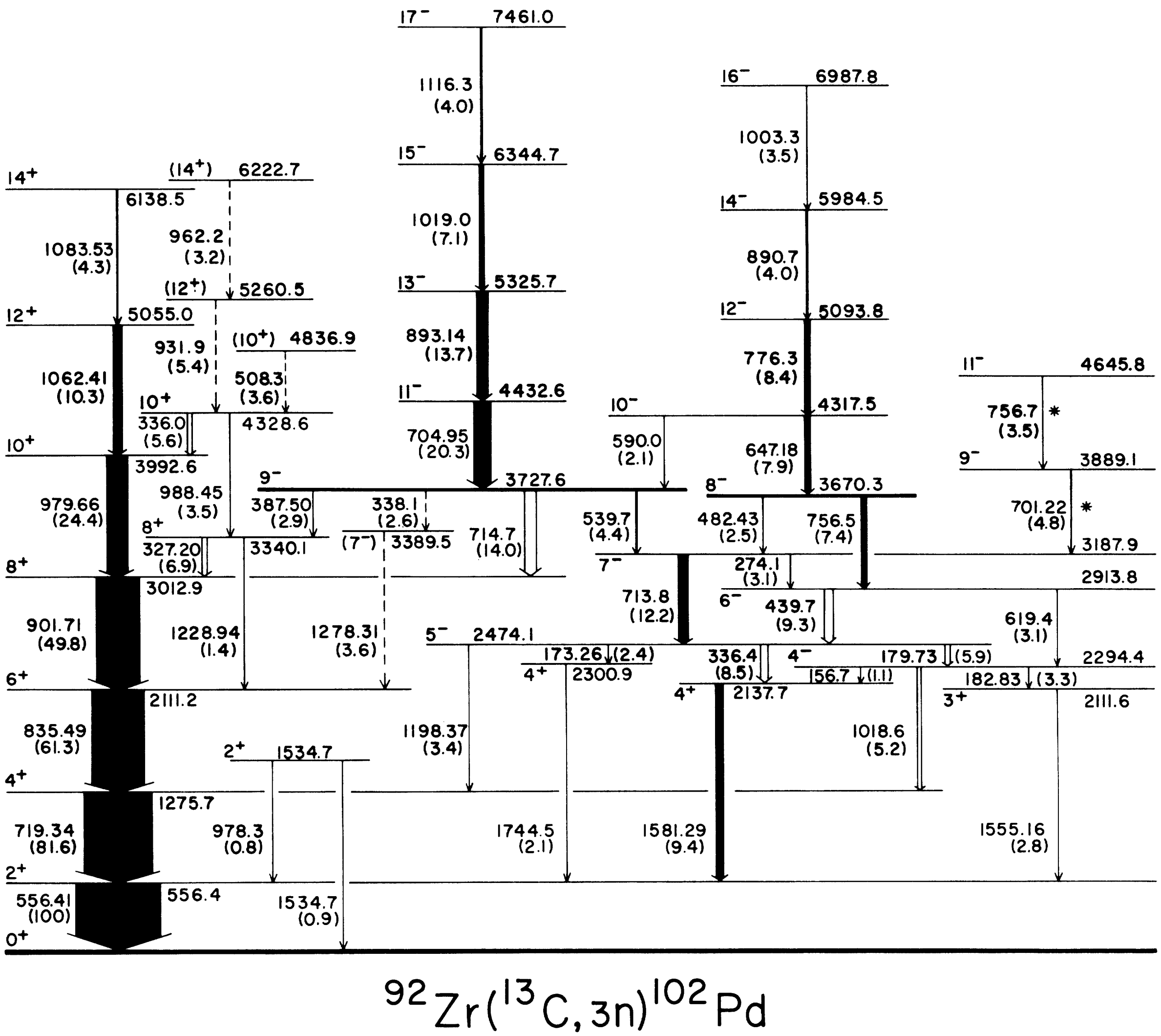

FIG. 6. Decay scheme for ^{102}Pd. Solid arrows indicate $E2$ transitions. Relative intensities are given in parentheses. The order suggested for the two levels indicated by * may be incorrect.

B. Angular momentum analysis

Table VIII lists angular distribution results for many of the γ rays assigned to ^{102}Pd. The 1003-, 1019-, and 1116-keV transitions have been assigned $\Delta I = -2$, $E2$ even though their angular distributions have been distorted by Doppler broadening.

Table IX lists average DCOQ ratios from the coincidence data for most of the transitions assigned to ^{102}Pd. Five $\Delta I = -1$ transitions with positive mixing ratios have been observed with DCOQ ratios near unity. These examples should emphasize that $R_{\mathrm{DCOQ}} = 1$ does not necessarily imply a $\Delta I = -2$, $L = 2$ transition. The mixing ratio determined from DCOQ for the 274-keV transition is more reliable than the δ determined from the angular distribution, because the 274-keV line contains 34% of unknown contamination in the singles spectra.

Seven $\Delta I = -1$, $E1$ transitions were observed in the ^{102}Pd data, all having the expected $R_{\mathrm{DCOQ}} \simeq 2$. Two of these transitions, the 336 and 715 keV, had nearly isotropic singles angular distributions due to strong contamination. The DCOQ data is especially crucial in this case since the interpretation of much of the data depends on the multipole character of these two transitions.[7]

The large number of $\Delta I = -2$, $E2$ transitions generally exhibit the expected $R_{\mathrm{DCOQ}} = 1$. Six of these transitions (540, 619, 714, 891, 932, and 1019 keV) were significantly contaminated in the singles data. Note especially that the 714-keV γ ray, which was unresolved from the 715-keV $E1$ γ ray, has been shown to have a positive A_{22}, thereby explaining the isotropic angular distribution of the 715-keV multiplet. Finally, the 156.7-, 336.0-, and 1018.6-keV transitions, which are significantly contaminated in the singles, are shown to be consistent with $\Delta I = 0$ assignments.

C. Linear polarization data

A linear polarization measurement on γ rays emitted following the $^{92}Zr(^{13}C, 3n\gamma)^{102}Pd$ reaction has been performed at Brookhaven National Laboratory.[24] The results of these measurements are more difficult to interpret because only one of the key parity-changing transitions could be measured without interference: the 387.5-keV γ ray was unambiguously assigned as $E1$. The 173.3- and 182.8-keV γ rays were too low in energy and the 1198.4-keV γ ray was too weak to be measured accurately. The 714.7- and 336.4-keV γ rays are badly contaminated in the singles spectra; however, as will be discussed below, they do provide useful information.

TABLE VIII. Angular distribution analysis for γ rays assigned to ^{102}Pd.

Energy	$I_i^\pi \to I_f^\pi$	A_{22}	A_{44}	α_2	α_4	Mixing ratio
173	$5^- \to 4^+$	−0.370(26)	0.05(3)	0.64(8)	0.30(17)	−0.12(4)
180	$5^- \to 4^-$	0.353(17)	−0.011(20)	0.64(8)	0.30(17)	0.47(6)
183	$4^- \to 3^+$	−0.260(21)	0.053(26)	0.57(10)	0.20(11)	−0.05(5)
274 [a]	$7^- \to 6^-$	0.037(23)	0.019(29)	0.67(8)	0.33(17)	0.17(2) [a]
327 [a]	$8^+ \to 8^+$	0.281(19)	−0.005(23)	0.70(5)	0.52(14)	−0.19(5) [a]
338	$9^- \to 7^-$	0.41(11)	−0.13(7)	0.97(26)	0.72(40)	
387	$9^- \to 8^+$	−0.43(5)	0.11(6)	0.73(5)	0.58(14)	−0.15(4)
440 [a]	$6^- \to 5^-$	0.214(20)	0.045(25)	0.67(8)	0.33(17)	0.32(3) [a]
482	$8^- \to 7^-$	0.57(6)	0.22(8)	0.71(8)	0.37(17)	1.6(7)
508 [a]	$10^+ \to 10^+$	0.06(3)	−0.08(4)	0.67(8)	0.54(20)	−0.66(10) [a]
540 [a]	$9^- \to 7^-$	0.191(19)	−0.055(25)	0.46(5)	0.30(14)	
556 [a]	$2^+ \to 0^+$	0.272(10)	−0.080(10)	0.38(2)	0.05(1)	
590	$10^- \to 9^-$	−0.20(6)	0.11(8)	0.74(5)	0.45(15)	0.01(4) or < −8
619 [a]	$6^- \to 4^-$	0.13(4)	−0.05(6)	0.29(9)	0.21(23)	
647	$10^- \to 8^-$	0.308(20)	−0.079(26)	0.74(5)	0.45(15)	
701	$9^- \to 7^-$	0.29(4)	−0.06(5)	0.68(9)	0.32(29)	
705	$11^- \to 9^-$	0.308(16)	−0.107(20)	0.75(4)	0.64(12)	
715 [b]	$9^- \to 8^+$	−0.29(5)	0.02(5)	0.73(4)	0.58(12)	−0.05(4)
719 [a]	$4^+ \to 2^+$	0.280(10)	−0.081(11)	0.55(2)	0.22(3)	
756 [a]	$8^- \to 6^-$ / $11^- \to 9^-$	0.279(22)	−0.100(30)	0.65(5)	0.51(15)	
776 [a]	$12^- \to 10^-$	0.326(21)	−0.131(27)	0.81(5)	0.81(17)	
835	$6^+ \to 4^+$	0.301(11)	−0.091(12)	0.66(2)	0.38(5)	
891 [a]	$14^- \to 12^-$	0.300(20)	−0.105(26)	0.76(5)	0.69(17)	
893	$13^- \to 11^-$	0.272(22)	−0.097(29)	0.68(6)	0.62(18)	
902	$8^+ \to 6^+$	0.287(12)	−0.085(13)	0.67(3)	0.43(7)	
932 [a]	$12^+ \to 10^+$	0.300(23)	−0.135(30)	0.74(6)	0.84(19)	
962 [a]	$14^+ \to 12^+$	0.19(3)	−0.04(5)	0.47(9)	0.25(31)	
980	$10^+ \to 8^+$	0.279(15)	−0.095(18)	0.67(4)	0.54(10)	
988	$10^+ \to 8^+$	0.19(5)	−0.02(8)	0.46(13)	0.10(43)	
1003 [c]	$16^- \to 14^-$	0.01(5)	−0.04(7)	0.02(13)	0.29(48)	
1019 [c]	$4^- \to 4^+$ / $15^- \to 13^-$	0.154(18)	−0.064(24)			
1062	$12^+ \to 10^+$	0.239(21)	−0.085(28)	0.59(5)	0.53(17)	
1084	$14^+ \to 12^+$	0.31(6)	0.00(8)	0.77(14)	0.00(51)	
1116 [c]	$17^- \to 15^-$	0.09(4)	0.07(6)	0.23(11)	−0.53(41)	
1198	$5^- \to 4^+$	−0.27(7)	−0.02(9)	0.64(8)	0.30(17)	−0.04(6)
1229	$8^+ \to 6^+$	0.10(10)	0.05(15)	0.23(24)	<0.47	
1278	$7^- \to 6^+$	−0.29(5)	−0.03(6)	0.70(6)	0.42(15)	−0.05(4)
1535	$2^+ \to 0^+$	0.13(19)	−0.11(27)	0.18(27)	0.06(16)	
1555	$3^+ \to 2^+$	0.07(6)	0.11(9)	0.51(10)	0.13(9)	0.24(6) or $\lvert\delta\rvert > 15$
1581	$4^+ \to 2^+$	0.306(24)	−0.10(3)	0.60(5)	0.27(9)	

[a] Uncorrected for contamination in singles spectra.
[b] Corrected for the presence of 46% $E2$ ($7^- \to 5^-$). Uncorrected values $A_{22} = 0.006(14)$, $A_{44} = -0.029(16)$.
[c] Possibly Doppler broadened.

TABLE IX. Average DCOQ ratios from the coincidence data for most of the transitions assigned to ^{102}Pd. Detector angles were 90° and −30°.

Energy	$I_i^\pi \to I_f^\pi$	R_{DCOQ}	Mixing ratio From DCO	Mixing ratio From AD
		$\Delta I=-1$ transitions with $\delta>0$		
179.73	$5^- \to 4^-$	0.96(9)	0.46(12)	0.47(6)
274.1 [a]	$7^- \to 6^-$	0.93(21)	0.48(21)	0.17(2) [a]
439.7 [a]	$6^- \to 5^-$	1.05(13)	0.39(13)	0.32(3) [a]
482.43	$8^- \to 7^-$	1.01(26)	5(5)	1.6(7)
1555.16	$3^+ \to 2^+$	1.3(4)	0.4(4) or $\lvert\delta\rvert>2.5$	0.24(16) or $\lvert\delta\rvert>15$
		$\Delta I=-1$ transitions with $\delta\simeq 0$		
173.26	$5^- \to 4^+$	1.9(7)	−0.09(30)	−0.12(4)
182.83	$4^- \to 3^+$	2.2(4)	−0.20(16)	−0.05(5)
336.4 [a]	$5^- \to 4^+$	1.96(28)	−0.06(9)	
387.50	$9^- \to 8^+$	1.80(17)	−0.05(7)	−0.15(4)
714.7 [a]	$9^- \to 8^+$	1.70(13)	0.01(6)	−0.05(4) [a]
1198.37	$5^- \to 4^+$	1.6(4)	0.10(20)	−0.04(6)
1278.31	$7^- \to 6^+$	2.0(8)	0.00(30)	−0.05(4)
		$\Delta I=-2, E2$ transitions		
539.7 [a]	$9^- \to 7^-$	1.02(18)		
556.41 [a]	$2^+ \to 0^+$	0.96(4)		
619.4 [a]	$6^- \to 4^-$	0.95(35)		
647.18	$10^- \to 8^-$	0.99(13)		
701.22	$9^- \to 7^-$	1.32(35)		
704.95	$11^- \to 9^-$	0.93(3)		
713.8 [a]	$7^- \to 5^-$	1.02(15)		
719.34 [a]	$4^+ \to 2^+$	1.05(5)		
756.5 [a]	$8^- \to 6^-$	0.77(17)		
756.7 [a]	$11^- \to 9^-$	0.78(28)		
776.3 [a]	$12^- \to 10^-$	0.88(13)		
835.49	$6^+ \to 4^+$	1.04(5)		
890.7 [a]	$14^- \to 12^-$	1.03(30)		
893.14	$13^- \to 11^-$	1.04(10)		
901.71	$8^+ \to 6^+$	1.01(5)		
931.9 [a]	$12^+ \to 10^+$	0.98(21)		
962.2 [a]	$14^+ \to 12^+$	0.64(22)		
979.66	$10^+ \to 8^+$	1.00(6)		
988.45	$10^+ \to 8^+$	1.5(6)		
1003.3 [a,b]	$16^- \to 14^-$	1.17(35)		
1019.0 [a,b]	$15^- \to 13^-$	1.23(19)		
1062.41	$12^+ \to 10^+$	1.12(12)		
1083.53	$14^+ \to 12^+$	0.95(23)		
1116.3 [b]	$17^- \to 15^-$	1.63(31)		
1228.94	$8^+ \to 6^+$	1.0(6)		
1581.29	$4^+ \to 2^+$	1.23(18)		
		Remaining transitions		
156.7 [a]	$4^- \to 4^+$	0.9(5)	1.5(21)	
327.20 [a]	$8^+ \to 8^+$	0.87(7)	0.0(5)	−0.19(5) [a]
336.0 [a]	$10^+ \to 10^+$	0.86(9)	0.0(7)	
508.3 [a]	$10^+ \to 10^+$	1.43(32)	<−0.4 or >1.0	−0.66(10) [a]
590.0	$10^- \to 9^-$	2.5(12)	−0.2(4) or <−1.3	0.01(4) or <−8
1018.6 [a]	$4^- \to 4^+$	0.95(23)	0.7(9)	

[a] Transition is contaminated in the singles spectra.
[b] Possibly Doppler broadened.

D. Discussion of the ^{102}Pd level scheme

The negative parity of the 9^- state is established by the linear polarization measurement[24] which shows that the 387.5-keV, 9^- to 8^+ transition changes parity while the 327-keV, 8^+ to 8^+ transition does not. The distinct $E2$ character of the 705- and 893-keV γ rays insures the negative parity of the 11^- and 13^- states.

As shown in Table VII, the 539.7-keV, 9^- to 7^- transition is badly contaminated by the 540.2-keV, $E2$ transition in ^{100}Ru. However, the DCOQ and the angular distribution data show that the 539.7-keV γ ray is also a quadrupole transition. The linear polarization[24] shows that if both transitions are quadrupole then neither can change parity, which establishes negative parity for the 3147.9-keV, 7^- state. The angular distribution shows that the 482.4-keV transition is a $\Delta I = -1$, highly mixed $E2/M1$ transition establishing the negative parity of the 8^- state. The distinct $E2$ character of the 647.2-, 776.3-, and 890.7-keV γ rays assures the negative parity of the 10^-, 12^-, and 14^- states.

The DCOQ results show that the A_{22} for the 336.4-keV γ ray must be negative while the A_{22} for the 336.0-keV γ ray must be positive. With these facts, the linear polarization[24] requires that the 5^- to 4^+ transition (336.4 keV) must be $E1$, assuring the negative parity of the 5^- state at 2474.1 keV. Even though the 439.7-keV γ ray is slightly contaminated in the singles spectra, its angular distribution assures that it is a $\Delta I = -1$, mixed $E2/M1$ transition which establishes the negative parity of the 6^- state. The data for the three 714-keV transitions is more complicated to interpret, but it confirms the change in parity between the 9^- and 8^+ states and no change in parity between the 7^- and 5^- states.

The 714-keV multiplet provides a good cross check of the assignments. The DCOQ measurements show that the 714.7-keV transition has a negative A_{22} while the 713.8-keV transition has a positive A_{22}. Then the linear polarization[24] requires that the two transitions must be $E1$ and $E2$. The attenuation coefficients for the 7^- state can be obtained from the three transitions that feed this state, so the distribution coefficients of the 713.8-keV transition can be calculated. These were subtracted from the combined angular distribution to get the coefficients of the 714.7-keV transitions. The small effect of the weak 714.0-keV, $E2$ ^{103}Pd γ ray was also included. As expected, the results indicate that the 714.7-keV transition is essentially pure dipole.

With one exception, the results from the decay[11] of the 5^+ isomer of ^{102}Ag agree with the positive-parity states presented here up to the 2300.9-keV level. Reference 11 assigns one state at 2111.5 keV to be 4^+, whereas we see a 6^+ state at 2111.2 keV and a 3^+ state at 2111.6 keV. Our assignments are in perfect agreement with their measurements but of course not with their conclusions.

VI. DISCUSSION

The most intense transitions have been collected in Fig. 7 to show the striking similarity in the collective structure of the three nuclei. There are both experimental and theoretical reasons to give special consideration to the 10^+, 9^-, and 8^- states. In ^{104}Pd the ground-state band is a normal quasirotational sequence up to the 8^+ level. (The term "quasirotational" is used to indicate that the γ-ray energies in a cascade increase monotonically as the angular momentum I increases.) However, the 10^+ to 8^+ transition has too small an energy for the 10^+ state to be a continuation of the ground-state band. A new quasirotational sequence begins at the 10^+ level with energy intervals quite similar to the lower levels in the ground-state band. This implies that the 12^+, 14^+, 16^+, and 18^+ states are the result of collective excitations of the core coupled to a 10^+ bandhead. There is a similar break in the energy level systematics at the 9^- and 8^- states. The energies of the 9^- to 7^- (380 keV) and 8^- to 6^- (251 keV) transitions are small compared to the 2^+ to 0^+ energy of the core (556 keV). Again we notice that the $E2$ γ rays above the 9^- and 8^- levels follow a regular quasirotational sequence indicating that the 9^- and 8^- states serve as bandheads.

Collective bands are also evident in the other two nuclei. The 10^+ state in ^{106}Pd is too low in energy to be a member of the ground-state band, and there seems to be a new quasirotational sequence beginning at the 10^+ level. In ^{102,106}Pd the energies of the states above 8^- and 9^- follow the regular quasirotational sequence exhibited by the core, whereas the 8^- to 6^- transition energies are clearly out of line, being too large (757 keV) in ^{102}Pd and too small (299 keV) in ^{106}Pd relative to the 10^- to 8^- transitions. The break at the 9^- level in ^{102,106}Pd is not as clear as it is in ^{104}Pd. With these general features of the nuclei in mind, we will next consider the interpretation provided by specific rotational and vibrational models.

A. Rotational model with Coriolis coupling

Superficially there seems to be little similarity between these Pd nuclei and typical strongly deformed nuclei; nevertheless, our experimental results are in excellent agreement with a rotational description of Pd. To understand this it is necessary to consider the differences between rotational

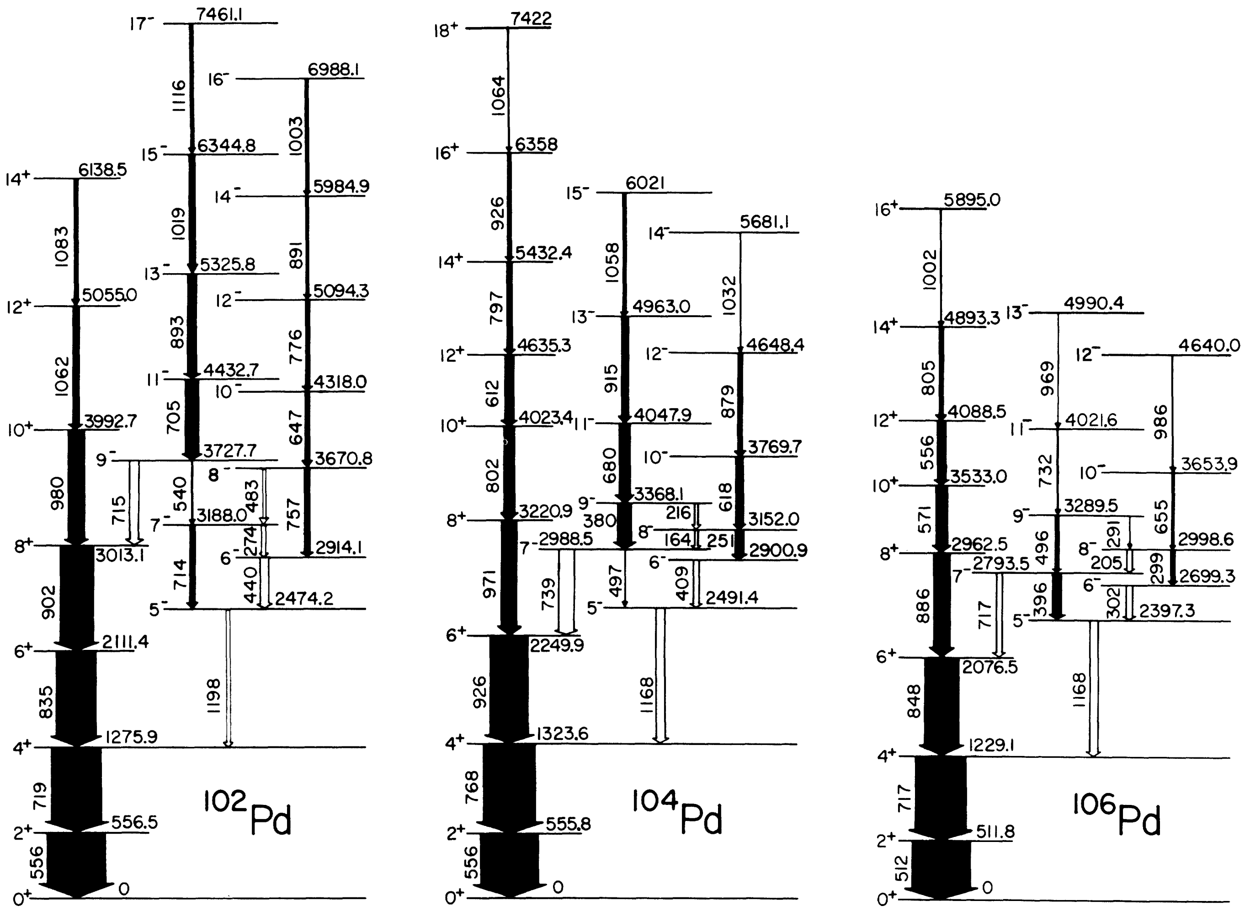

FIG. 7. Simplified decay schemes showing the most intense transitions in $^{102,104,106}Pd$.

states in strongly deformed and slightly deformed nuclei.

The large angular frequency ω which a slightly deformed nucleus must attain to produce even a fairly small amount of angular momentum has two significant consequences. The first is that Coriolis effects, being proportional to ω, are expected to be large. For the even-even nuclei this manifests itself as a tendency for normally paired nucleons to break up and align with the core angular momentum. The second consequence of large ω is a significant increase in the apparent moment of inertia, which is noticeable even at the lowest of spins. If due to either centrifugal stretching or Coriolis antipairing, both of which should have significant effects at high values of ω, this variable moment of inertia is readily understandable and must be included in any theoretical treatment of slightly deformed rotors. Smith and Rickey[25] have found this to be the case in a Coriolis-coupling calculation for odd-neutron Pd nuclei.

Stephens[26] has shown that if the Coriolis effects are strong enough, a coupling scheme emerges in which J, α, and R are good quantum numbers, J being the total particle angular momentum, α the projection of J onto the total spin I, and R the angular momentum of the core. In this scheme the yrast states are said to be "decoupled." They will have $\alpha = J$, and for $I \geq J$ the energy spacings follow those of the core for $R = 0$, 2, 4, etc.; that is, $R(R+1)$-type rotational bands will feed states of maximum J. (This is in contrast to the $I(I+1)$-type bands seen in strongly deformed nuclei.)

This interpretation is in good qualitative agreement with the even-A Pd data. In this region the $d_{5/2}$, $g_{7/2}$, and $h_{11/2}$ single-neutron orbitals are expected to be available, and appropriate combinations of these orbitals will produce maximum two-quasiparticle spins of $J = 10^+$, 9^-, and 8^-. As discussed above, states of these spins do indeed appear to serve as bandheads for rotational excitations in $^{102,104,106}Pd$.

The Stephens model has been widely applied to odd-A nuclei for particles of high spin and unique parity, for which cases the particle spin j is a very good quantum number; however, there has not been much supportive data for the analogous two-quasiparticle configuration of even-A nuclei. The mutual alignment of the two particles introduces an extra degree of freedom in the even-A case, therefore it may not be valid to assume sharp J values. While the dominant J of the yrast states may be $J=j_1+j_2$, other J values will probably mix in to cause a departure from the simple particle-plus-core description.

To fully understand this data in terms of a rotational description it will be necessary to perform an exact diagonalization of the Hamiltonian including all of the two-quasiparticle basis states which might Coriolis mix together. Flaum and Cline[27] have done a preliminary calculation on ^{104}Pd which is in good agreement with our data, even though there are several refinements which could be made: the addition of several basis states, which had been left out to minimize computer time, might affect the calculation, and use of the same deformation, Nilsson single-particle energies, and type of variable-moment-of-inertia treatment used successfully by Smith and Rickey[25] for the odd-A Pd nuclei would probably improve the results. Even without these refinements, the average energy difference between theory and experiment for the 11 negative-parity states from 5^- to 15^- is only 43 keV. The calculation indicated a considerable amount of J mixing so that the simple interpretation of maximally aligned two-quasiparticle bands should be regarded only as a first-order description, or perhaps the "dominant component" of the true description.

It would be worthwhile to extend the ^{104}Pd calculation to ^{102,106}Pd because one of the crucial tests of the model should be whether or not the systematics displayed by ^{102,104,106}Pd can be reproduced by simply changing the Fermi level. The following observations must be explained. (1) The 8^-, 9^-, and 10^+ two-quasiparticle states all drop in energy with increasing neutron number. (2) The odd-even splitting of the negative-parity states increases with the neutron number. (3) In addition to the yrast negative-parity states many other negative-parity states are observed in ^{106}Pd. (4) The character of the 7^- state appears to have changed dramatically in going from ^{104}Pd to ^{106}Pd, as evidenced by a factor of 33 decrease in the ratio $B(E1,\ 7^- \rightarrow 6^+)/B(E2,\ 7^- \rightarrow 5^-)$. (5) In ^{102}Pd, $B(E1,\ 5^- \rightarrow 4^+)$ is over 100 times larger for the higher 4^+ states than for the ground-state-band 4^+ state, while in ^{104}Pd these are essentially equal and in ^{106}Pd the overlap with the ground-state-band 4^+ has become the larger, by at least a factor of 3.

Only the first of these observations is readily understandable. With increasing neutron number the Fermi level moves closer to the $h_{11/2}$ orbitals and since these orbitals are presumed to contribute to all of the two-quasiparticle states, one would expect these states to systematically drop in energy. The last two observations could be related to the rotational content of the 7^- and 5^- states. For example, we would expect $B(E1,\ 7^- \rightarrow 6^+)$ to be related to the amount of $R=6$ mixing in the 7^- state. One should look for a systematic change in the amount of this mixing when future calculations are performed.

In the absence of a complete two-quasiparticle-plus-core calculation for ^{102,104,106}Pd it is instructive to consider the observed[1,4,5,28] systematic behavior of the adjacent odd-A nuclei ^{101,103,105}Pd. We know from observation that in the yrast configuration the $h_{11/2}$ odd particle decouples from the even-A Pd core. An additional decoupled $h_{11/2}$ particle could combine with the $\frac{11}{2}^-$, $\frac{7}{2}^+$, and $\frac{5}{2}^+$ bands observed in ^{101,103,105}Pd to produce the 10^+, 9^-, and 8^- bands in ^{102,104,106}Pd. In applying this picture we notice that just as ^{101}Pd exhibits two strongly fed $\Delta I=2$ bands built on the $\frac{5}{2}^+$and $\frac{7}{2}^+$ states, ^{102}Pd has two well-formed $\Delta I=2$ bands feeding the 8^- and 9^- states. In ^{105}Pd, however, many additional positive-parity states are fed, and the corresponding negative-parity states are observed in ^{106}Pd. Just as the $\frac{5}{2}^+$ band in ^{105}Pd is a $\Delta I=1$ band, a cascade of dipoles (463, 413, and 385 keV) is observed to feed the 8^- state in ^{106}Pd. The observed trend toward an increase in the odd-even splitting of the negative-parity states in ^{102,104,106}Pd is reminiscent of the increased splitting of the "favored" and "unfavored" members of the $\frac{5}{2}^+$ and $\frac{7}{2}^+$ bands in ^{101,103,105}Pd. This suggests that the even-spin, negative-parity states might have large components from higher K values, in analogy to the higher K values of the unfavored states in the odd-A nuclei. Such an interpretation has also been suggested from the calculations of Flaum and Cline[27] on ^{104}Pd. The 11^- state, for example, was mostly $K=0$ and $K=1$, whereas the 10^- state had large contributions from $K=2$ and $K=3$.

B. Interacting boson vibrational description

Iachello and Arima[29] have proposed that collective excitations in "vibrational" nuclei can be described in an interacting boson approximation (IBA). In this picture the ground-state band and the low-lying, positive-parity states are produced by quadrupole bosons. The interaction between these bosons would account for the deviations from the simple vibrational description that are observed experimentally—i.e., the progressive increase in the energy spacing of the ground-state band and the breaking of degeneracy of the vibrational multiplets. As is usually the case, little is learned by just considering the ground-state band. The IBA gives a satisfactory fit to the ground-state band but so does the variable-moment-of-inertia (VMI) model.[30]

The predictions made for the lower-spin states in a multiplet provide a much more interesting test for IBA. The displacement of these states from the corresponding members of the ground-state band is given by simple relations:

$$E(n=2,\ I=4)-E(n=2,\ I=2)=C_4-C_2\ ,$$

$$E(n=3,\ I=6)-E(n=3,\ I=3)=2.14\ (C_4-C_2)\ ,$$

$$E(n=3,\ I=6)-E(n=3,\ I=4)=1.571\ (C_4-C_2)\ ,$$

where n is the number of phonons present, C_2 and C_4 are parameters which characterize the interaction between the phonons, and I is the total angular momentum. The parameter C_4 can be fixed by fitting the energy levels of the ground-state band, and C_2 is selected to agree with the energy of the $I=2'$, 3, and $4'$ states.

It is evident from these expressions that the multiplets are degenerate if $C_2=C_4$. If $C_2\neq C_4$, *all* three states must be above ($C_2>C_4$) or below ($C_2<C_4$) the corresponding member of the ground-state band. This condition is not met for ^{102,104}Pd. In ^{102}Pd the $2^{+\prime}$ state is 260 keV above the 4^+ member of the ground-state band, while the 3^+ and 6^+ states have the same energy. The IBA approximation would place the 3^+ state 556 keV above the 6^+ state. Of course, it is possible that such a state is present, and it is not observed in this experiment because it is far above the yrast line. In ^{104,106}Pd, the observed 3^+ state is much too low in energy to be consistent with the observed $2^{+\prime}$ and $4^{+\prime}$ states. Thus the low-spin, positive-parity states seen in these experiments do not seem to be in agreement with the first-order predictions of the IBA. (By contrast the predictions of the asymmetric rotor model,[31] $E(3^+)=E(2^{+\prime})+E(2^+)$ and $E(4^{+\prime})\simeq E(6^+)$, agree quite well with the data for all three nuclei.)

Iachello and Arima[32] have suggested that negative-parity states could be treated in IBA by including quadrupole and octopole bosons. Three new parameters are needed to describe the energy of the octopole phonon and its interactions. The agreement with the energy of the negative-parity states is not as good as it is for the ground-state band. This is especially true in ^{104}Pd, where the IBA does not reproduce the compression of the 7^-, 6^-, and 5^- states as well as the rotational calculation of Flaum and Cline[27] does.

One of the merits of the IBA approach is that it gives simple expressions for $B(E2)$ values so that branching ratios for $E2$ transitions can be calculated. The most important result is that the $E2$ branching ratio $P(\Delta I=-1)/P(\Delta I=-2)$ should be approximately zero if the initial angular momentum is odd [e.g., (9^- to 8^-)/9^- to 7^-)] and the ratio should be very small if the initial angular momentum is even [e.g., (8^- to 7^-)/(8^- to 6^-)]. In order to compare these predictions to our data, the measured mixing ratios must be used to extract the $E2$ component of $\Delta I=-1$ transitions.

Our results do not agree with this feature of the IBA. The (6^- to 5^-)/(6^- to 4^-) ratio is approximately 5, 6, and 17 times larger than expected in ^{102,104,106}Pd, respectively. The (8^- to 7^-)/(8^- to 6^-) ratio is 14, 7, and 1.5 times the predicted value in ^{102,104,106}Pd, respectively. In ^{106}Pd the 11^- to 10^- and 9^- to 8^- transition intensities are orders of magnitude larger than expected.

Collective bands built on two-quasiparticle states have been observed[33,3] in even-even Ba and Pt nuclei. However, the even-spin, negative-parity states were not observed, so an octopole description of those nuclei can not be excluded.

C. Summary

These experiments provide ample evidence that the yrast states populated in (HI,xn) reactions are in good agreement with a slightly deformed-rotor description of these nuclei. The dominant features can be interpreted as four collective bands built on the ground state and three excited two-quasiparticle states. The spin and parity of these bandheads are just that expected from the decoupled bands observed in odd-A Pd nuclei. The excited bands and the lower-energy, negative-parity states can be understood qualitatively on the basis of the Coriolis alignment model of Stephens.[2] Furthermore, Flaum and Cline[27] have found excellent agreement between the ^{104}Pd level scheme and a complete Coriolis-coupling calculation.

The IBA of Iachello and Arima[29] is an attractive approach because it gives the general features of the energy levels from a very simple calculation. However, it is much less successful when it comes to interpreting lower-spin members from "vibrational" multiplets or branching ratios in the negative-parity bands.[32]

*Research supported by the National Science Foundation.
†Current address: Brookhaven National Laboratory, Upton, New York 11973.

[1]F. A. Rickey and P. C. Simms, Phys. Rev. Lett. 31, 404 (1973).
[2]F. S. Stephens, Rev. Mod. Phys. 47, 43 (1975).
[3]M. Pipparinen, J. C. Cunnane, P. J. Daly, C. L. Dors, F. M. Bernthal, and T. L. Khoo, Phys. Rev. Lett. 34, 1110 (1975).
[4]P. C. Simms, G. J. Smith, F. A. Rickey, J. A. Grau, J. R. Tesmer, and R. M. Steffen, Phys. Rev. C 9, 684 (1974).
[5]J. A. Grau, F. A. Rickey, G. J. Smith, P. C. Simms, and J. R. Tesmer, Nucl. Phys. A229, 346 (1974).
[6]P. C. Simms, R. Anderson, F. A. Rickey, G. Smith, R. M. Steffen, and J. R. Tesmer, Phys. Rev. C 7, 1631 (1973).
[7]J. A. Grau, Z. W. Grabowski, F. A. Rickey, P. C. Simms, and R. M. Steffen, Phys. Rev. Lett. 32, 677 (1974).
[8]G. Scharff-Goldhaber, M. McKeown, A. H. Lumpkin, and W. F. Piel, Jr., Phys. Lett. 44B, 416 (1973).
[9]S. Cochavi, M. McKeown, O. C. Kistner, and G. Scharff-Goldhaber, J. Phys. (Paris) 33, No. 8-9, 102 (1972).
[10]E. P. Grigorev, A. V. Zolotavin, K. Ryde, and V. O. Sergeev, Bull. Acad. Sci. USSR Phys. Ser. 36, 63 (1973).
[11]D. J. Hnatowich, F. Münnich, and A. Kjelberg, Nucl. Phys. A178, 111 (1971).
[12]F. Münnich, A. Kjelberg, and D. J. Hnatowich, Nucl. Phys. A178, 97 (1971).
[13]K. Okano, Y. Kawase, and S. Uehara, Nucl. Phys. A182, 131 (1972).
[14]N. C. Singhal, N. R. Johnson, E. Eichler, and J. H. Hamilton, Phys. Rev. C 5, 948 (1972).
[15]P. Weight, P. Herzog, B. Richter, H. Hubel, H. Toschinski, and J. Fechner, Nucl. Phys. A122, 577 (1968).
[16]H. Inoue, J. Phys. Soc. Jpn. 35, 957 (1973).
[17]F. T. Avignone, III, and J. E. Pinkerton, Phys. Rev. C 7, 1238 (1973).
[18]K. S. Krane, R. M. Steffen, and R. M. Wheeler, Nucl. Data A11, 351 (1973).
[19]D. E. Raeside, Nucl. Instrum. Methods 87, 7 (1970).
[20]D. H. White, R. E. Birkett, and T. Thomson, Nucl. Instrum. Methods 77, 261 (1970).
[21]W. Beer and J. Kern, Nucl. Instrum. Methods 117, 183 (1974).
[22]D. C. Stromswold, D. O. Elliott, Y. K. Lee, J. A. Grau, L. E. Samuelson, F. A. Rickey, and P. C. Simms, Phys. Rev. C 13, 1510 (1976).
[23]K. S. Krane and R. M. Steffen, Phys. Rev. C 2, 724 (1970).
[24]D. C. Stromswold, D. Elliott, Y. K. Lee, W. F. Piel, Jr., and A. W. Sunyar, Johns Hopkins University Progress Report No. C-00-3274-18 (unpublished).
[25]H. A. Smith and F. A. Rickey, Phys. Rev. C 14, 1946 (1976).
[26]F. S. Stephens, R. M. Diamond, and S. G. Nilsson, Phys. Lett. 44B, 429 (1973).
[27]C. Flaum and D. Cline, University of Rochester Report No. UR-NSRL-103 (unpublished); and private communications.
[28]F. A. Rickey, J. A. Grau, L. E. Samuelson, and P. C. Simms, Phys. Rev. C (to be published).
[29]F. Iachello and A. Arima, Phys. Lett. 53B, 309 (1974).
[30]M. A. J. Mariscotti, Gertrude Scharff-Goldhaber, and B. Buck, Phys. Rev. 178, 1864 (1969).
[31]A. S. Davydov and A. A. Chaban, Nucl. Phys. 20, 499 (1960).
[32]F. Iachello and A. Arima (unpublished).
[33]C. Flaum, D. Cline, A. W. Sunyar, and O. C. Kistner, Phys. Rev. Lett. 33, 973 (1974).